

Fundamental limits on the rate of bacterial cell division

Nathan M. Belliveau^{†, 1}, Griffin Chure^{†, 2, 3}, Christina L. Hueschen⁴, Hernan G. Garcia⁵, Jané Kondev⁶, Daniel S. Fisher⁷, Julie Theriot^{1, 8}, Rob Phillips^{2, 9,*}

*For correspondence:

[†]These authors contributed equally to this work

¹Department of Biology, University of Washington, Seattle, WA, USA; ²Division of Biology and Biological Engineering, California Institute of Technology, Pasadena, CA, USA; ³Department of Applied Physics, California Institute of Technology, Pasadena, CA, USA; ⁴Department of Chemical Engineering, Stanford University, Stanford, CA, USA; ⁵Department of Molecular Cell Biology and Department of Physics, University of California Berkeley, Berkeley, CA, USA; ⁶Department of Physics, Brandeis University, Waltham, MA, USA; ⁷Department of Applied Physics, Stanford University, Stanford, CA, USA; ⁸Allen Institute for Cell Science, Seattle, WA, USA; ⁹Department of Physics, California Institute of Technology, Pasadena, CA, USA; *Contributed equally

Abstract This will be written next (promise).

Introduction

The range of bacterial growth rates is enormously diverse. In natural environments, some microbial organisms might double only once per year while in comfortable laboratory conditions, growth can be rapid with several divisions per hour. This six order of magnitude difference illustrates the intimate relationship between environmental conditions and the rates at which cells convert nutrients into new cellular material – a relationship that has remained a major topic of inquiry in bacterial physiology for over a century (*Jun et al., 2018*). As was noted by Jacques Monod, “the study of the growth of bacterial cultures does not constitute a specialized subject or branch of research, it is the basic method of Microbiology.” Those words ring as true today as they did when they were written 70 years ago. Indeed, the study of bacterial growth has undergone a molecular resurgence since many of the key questions addressed by the pioneering efforts in the middle of the last century can be revisited by examining them through the lens of the increasingly refined molecular census that is available for bacteria such as the microbial workhorse *Escherichia coli*. Several of the outstanding questions that can now be studied about bacterial growth include: what sets the fastest time scale that bacteria can divide, and how is growth rate tied to the quality of the carbon source. In this paper, we address these two questions from two distinct angles. First, as a result of an array of high-quality proteome-wide measurements of the *E. coli* proteome under a myriad of different growth conditions, we have a census that allows us to explore how the number of key molecular players change as a function of growth rate. This census provides a window onto whether the processes they mediate such as molecular transport into the cells and molecular synthesis within cells can run faster. Second, because of our understanding of the molecular pathways responsible for many of the steps in bacterial growth, we can also make order of magnitude estimates to infer the copy numbers that would be needed to achieve a given growth rate. In this paper, we pass back and forth between the analysis of a variety of different proteomic datasets and order-of-magnitude estimations to determine possible molecular bottlenecks that limit bacterial growth and to see how

42 the growth rate varies in different carbon sources.

43 Specifically, we leverage a combination of *E. coli* proteomic data sets collected over the past
 44 decade using either mass spectrometry (*Schmidt et al., 2016; Peebo et al., 2015; Valgepea et al.,*
 45 **2013**) or ribosomal profiling (*Li et al., 2014*) across 31 unique growth conditions. Broadly speaking,
 46 we entertain several classes of hypotheses as are illustrated in **Figure 1**. First, we consider potential
 47 limits on the transport of nutrients into the cell. We address this hypothesis by performing an
 48 order-of-magnitude estimate for how many carbon, phosphorous, and sulfur atoms are needed to
 49 facilitate this requirement given a 5000 second division time. As a second hypothesis, we consider
 50 the possibility that there exists a fundamental limit on how quickly the cell can generate ATP. We
 51 approach this hypothesis from two angles, considering how many ATP synthase complexes must
 52 be needed to churn out enough ATP to power protein translation followed by an estimation of
 53 how many electron transport complexes must be present to maintain the proton motive force.
 54 A third class of estimates considers the need to maintain the size and shape of the cell through
 55 the construction of new lipids for the cell membranes as well as the glycan polymers which make
 56 up the rigid peptidoglycan. Our final class of hypotheses centers on the synthesis of a variety of
 57 biomolecules. Our focus is primarily on the stages of the central dogma as we estimate the number
 58 of protein complexes needed for DNA replication, transcription, and protein translation.

59 In broad terms, we find that the majority of these estimates are in close agreement with the
 60 experimental observations, with protein copy numbers apparently well-tuned for the task of cell
 61 doubling. This allows us to systematically scratch off the hypotheses diagrammed in **Figure 1** as
 62 setting potential growth bottlenecks. Ultimately, we find that protein translation (particularly the
 63 generation of new ribosomes) acts as 1) a rate limiting step for the *fastest* bacterial division, and
 64 2) a major determinant of bacterial growth across the nutrient conditions we have considered
 65 under steady state, exponential growth. This perspective is consistent with the linear correlation
 66 observed between growth rate and ribosomal content (typically quantified through the ratio of RNA
 67 to protein) for fast growing cells (*Scott et al., 2010*), but also suggest a more prominent role for
 68 ribosomes in governing the changes in cell size and doubling time across all conditions of nutrient
 69 limitation.

70 Uptake of Nutrients

71 In order to build new cellular mass, the molecular and elemental building blocks must be scavenged
 72 from the environment in different forms. Carbon, for example, is acquired via the transport of
 73 carbohydrates and sugar alcohols with some carbon sources receiving preferential treatment
 74 in their consumption (*Monod, 1947*). Phosphorus, sulfur, and nitrogen, on the other hand, are
 75 harvested primarily in the forms of inorganic salts, namely phosphate, sulfate, and ammonia
 76 (*Jun et al., 2018; Assentoft et al., 2016; Stasi et al., 2019; Antonenko et al., 1997; Rosenberg et al.,*
 77 **1977; Willsky et al., 1973**). All of these compounds have different permeabilities across the cell
 78 membrane *Phillips (2018)* and most require some energetic investment either via ATP hydrolysis
 79 or through the proton electrochemical gradient to bring the material across the hydrophobic cell
 80 membrane. Given the diversity of biological transport mechanisms and the vast number of inputs
 81 needed to build a cell, we begin by considering transport of some of the most important cellular
 82 ingredients: carbon, nitrogen, oxygen, hydrogen, phosphorus, and sulfur.

83 The elemental composition of *E. coli* has received much quantitative attention over the past
 84 half century (*Neidhardt et al., 1991; Taymaz-Nikerel et al., 2010; Heldal et al., 1985; Bauer and Ziv,*
 85 **1976**), providing us with a starting point for estimating the copy numbers of various transporters.
 86 While there is some variability in the exact elemental percentages (with different uncertainties), we
 87 can estimate that the dry mass of a typical *E. coli* cell is \approx 45% carbon (BNID: 100649, *Milo et al.*
 88 (**2010**)), \approx 15% nitrogen (BNID: 106666, *Milo et al. (2010)*), \approx 3% phosphorus (BNID: 100653, *Milo*
 89 *et al. (2010)*), and 1% sulfur (BNID: 100655, *Milo et al. (2010)*). In the coming paragraphs, we will
 90 engage in a dialogue between back-of-the-envelope estimates for the numbers of transporters
 91 needed to facilitate these chemical stoichiometries and the experimental proteomic measurements

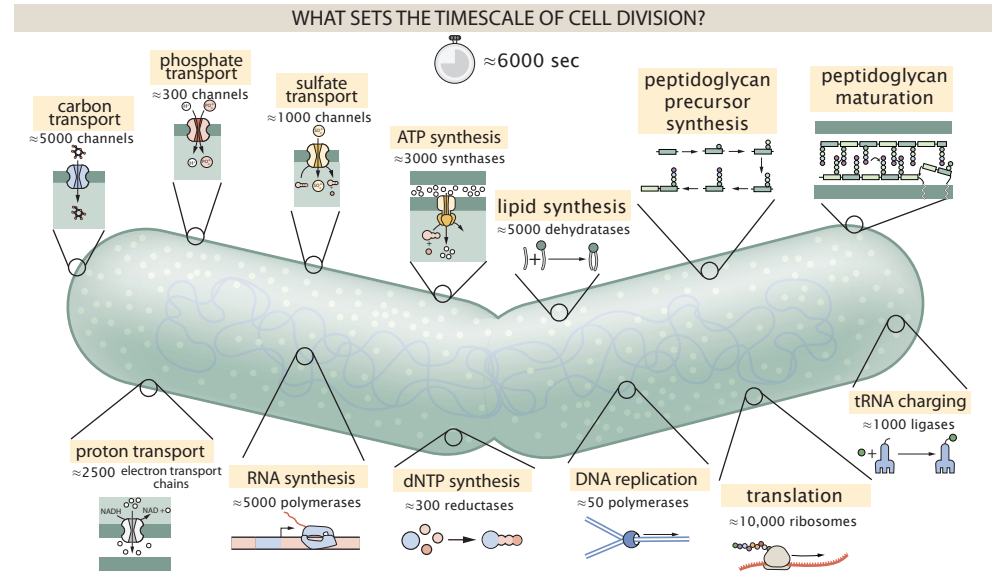


Figure 1. Transport and synthesis processes necessary for cell division. We consider an array of processes necessary for a cell to double its molecular components. Such processes include the transport of carbon across the cell membrane, the production of ATP, and fundamental processes of the central dogma namely RNA, DNA, and protein synthesis. A schematic of each synthetic or transport category is shown with an approximate measure of the complex abundance at a growth rate of 0.5 per hour. In this work, we consider a standard bacterial division time of ≈ 5000 sec.

of the biological reality. Such an approach provides the opportunity to test if our biological knowledge is sufficient to understand the scale at which these complexes are produced. Specifically, we will make these estimates considering a modest doubling time of 5000 s, a growth rate of $\approx 0.5 \text{ hr}^{-1}$, the range in which the majority of the experimental measurements reside.

Nitrogen Transport

Before we begin our back-of-the-envelope estimations, we must address which elemental sources must require proteinaceous transport, meaning that the cell cannot acquire appreciable amounts simply via diffusion from the membrane. The permeability of the lipid membrane to a large number of solutes has been extensively characterized over the past century. Large, polar molecular species (such as various sugar molecules, sulfate, and phosphate) have low permeabilities while small, non-polar compounds (such as oxygen, carbon dioxide, and ammonia) can readily diffuse across the membrane. Ammonia, a primary source of nitrogen in typical laboratory conditions, has a permeability on par with water ($\approx 10^5 \text{ nm/s}$, BNID:110824 *Milo et al. (2010)*). In particularly nitrogen-poor conditions, *E. coli* expresses a transporter (AmtB) which appears to aid in nitrogen assimilation, though the mechanism and kinetic details of transport is still a matter of debate (*van Heeswijk et al., 2013; Khademi et al., 2004*). Beyond ammonia, another plentiful source of nitrogen come in the form of glutamate, which has its own complex metabolism and scavenging pathways. However, nitrogen is plentiful in the growth conditions examined in this work, permitting us to neglect nitrogen transport as a potential rate limiting process in cell division in typical experimental conditions. We direct the reader to the supplemental information for a more in-depth discussion of permeabilities and a series of calculations revealing that active nitrogen transport can be neglected for the purposes of this article.

Carbon Transport

We begin our estimations with the most abundant element in *E. coli* by mass, carbon. Using $\approx 0.3 \text{ pg}$ as the typical *E. coli* dry mass (BNID: 103904, *Milo et al. (2010)*), we estimate that $\approx 10^{10}$ carbon atoms must be brought into the cell in order to double all of the carbon-containing

118 molecules (**Figure 2(A, top)**). Typical laboratory growth conditions, such as those explored in the
 119 aforementioned proteomic data sets, provide carbon as a single class of sugar such as glucose,
 120 galactose, or xylose to name a few. *E. coli* has evolved myriad mechanisms by which these sugars can
 121 be transported across the cell membrane. One such mechanism of transport is via the PTS system
 122 which is a highly modular system capable of transporting a diverse range of sugars (**Escalante et al., 2012**).
 123 The glucose-specific component of this system transports ≈ 200 glucose molecules per second per transporter (BNID: 114686, **Milo et al. (2010)**). Making the assumption that this is a
 124 typical sugar transport rate, coupled with the need to transport 10^{10} carbon atoms, we arrive at the
 125 conclusion that on the order of 1,000 transporters must be expressed in order to bring in enough
 126 carbon atoms to divide in 5000 s, diagrammed in the top panel of **Figure 2(A)**. This estimate, along
 127 with the observed average number of the PTS system carbohydrate transporters present in the
 128 proteomic data sets (**Schmidt et al., 2016; Peebo et al., 2015; Valgepea et al., 2013; Li et al., 2014**),
 129 is shown in **Figure 2(A)**. While we estimate 1500 transporters are needed with a 5000 s division
 130 time, we can abstract this calculation to consider any particular growth rate given knowledge of
 131 the cell density and volume as a function of growth rate and direct the reader to the SI for more
 132 information. As revealed in **Figure 2(A)**, experimental measurements exceed the estimate by several
 133 fold, illustrating that transport of carbon in to the cell is not rate limiting for cell division. Abstracting
 134 this point estimate at 5000 s to a continuum of growth rates (grey line in **Figure 2(A)**) reveals an
 135 excess of transporters at other growth rates, though in rapid growth regimes, the abundance is
 136 below our simple estimate.
 137

138 The estimate presented in **Figure 2(A)** neglects any specifics of the regulation of carbon transport
 139 system and presents a data-averaged view of how many carbohydrate transporters are present
 140 on average. Using the diverse array of growth conditions explored in the proteomic data sets, we
 141 can explore how individual carbon transport systems depend on the population growth rate. In
 142 **Figure 2(B)**, we show the total number of carbohydrate transporters specific to different carbon
 143 sources. A striking observation, shown in the top-left plot of **Figure 2(B)**, is the constancy in the
 144 expression of the glucose-specific transport systems. Additionally, we note that the total number
 145 of glucose-specific transporters is tightly distributed $\approx 10^4$ per cell, the approximate number of
 146 transporters needed to sustain rapid growth of several divisions per hour. This illustrates that *E. coli*
 147 maintains a substantial number of complexes present for transporting glucose which is known
 148 to be the preferential carbon source (**Monod, 1947; Liu et al., 2005; Aidelberg et al., 2014**).

149 It is now understood that a large number of metabolic operons are regulated with dual-input
 150 logic gates that are only expressed when glucose concentrations are low (mediated by cyclic-AMP
 151 receptor protein CRP) and the concentration of other carbon sources are elevated (**Gama-Castro et al., 2016; Zhang et al., 2014b**). A famed example of such dual-input regulatory logic is in the
 152 regulation of the *lac* operon which is only natively activated in the absence of glucose and the
 153 presence of allolactose, an intermediate in lactose metabolism (**Jacob and Monod, 1961**), though we
 154 now know of many other such examples (**Ireland et al., 2020; Gama-Castro et al., 2016; Belliveau et al., 2018**). This illustrates that once glucose is depleted from the environment, cells have a means
 155 to dramatically increase the abundance of the specific transporter needed to digest the next sugar
 156 that is present. Several examples of induced expression of specific carbon-source transporters
 157 are shown in **Figure 2(B)**. Points colored in red (labeled by red text-boxes) correspond to growth
 158 conditions in which the specific carbon source (glycerol, xylose, or fructose) is present. These
 159 plots show that, in the absence of the particular carbon source, expression of the transporters
 160 is maintained on the order of $\sim 10^2$ per cell. However, when the transport substrate is present,
 161 expression is induced and the transporters become highly-expressed. The grey lines in **Figure 2(B)**
 162 show the estimated number of transporters needed at each growth rate to satisfy the cellular
 163 carbon requirement. It is notable that in all cases, the magnitude of induced expression (shown in
 164 red) falls close to the estimate, illustrating the ability of the cell to tune expression in response to
 165 changing environments. Together, this generic estimation and the specific examples of induced
 166 expression suggest that transport of carbon across the cell membrane, while critical for growth, is
 167 168

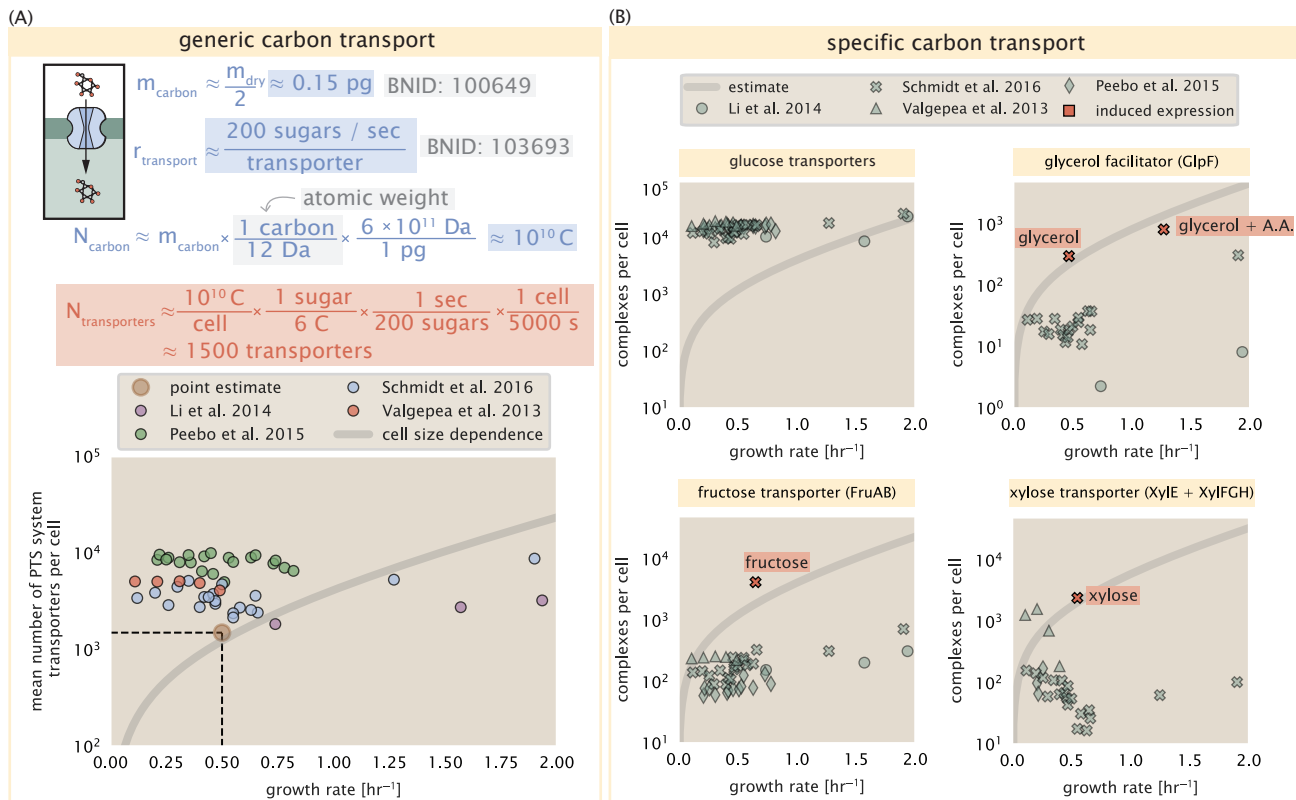


Figure 2. The abundance of carbon transport systems across growth rates. (A) A simple estimate for the minimum number of generic carbohydrate transport systems (top) assumes $\approx 10^{10}$ C are needed to complete division, each transported sugar contains ≈ 6 C, and each transporter conducts sugar molecules at a rate of ≈ 200 per second. Bottom plot shows the estimated number of transporters needed at a growth rate of ≈ 0.5 per hr (light-brown point and dashed lines). Colored points correspond to the mean number of PTS system sugar transporters (complexes annotated with the Gene Ontology term GO:0009401) for different growth conditions across different published datasets. (B) The abundance of various specific carbon transport systems plotted as a function of the population growth rate. The rates of substrate transport to compute the continuum growth rate estimate (grey line) were 200 glucose·s⁻¹ (BNID: 103693, *Milo et al. (2010)*), 2000 glycerol·s⁻¹ (*Lu et al., 2003*), 200 fructose·s⁻¹ (assumed to be similar to PtsI, BNID: 103693, *Milo et al. (2010)*), and 50 xylose·s⁻¹ (assumed to be comparable to LacY, BNID:103159, *Milo et al. (2010)*). Red points and highlighted text indicate conditions in which the only source of carbon in the growth medium induces expression of the transport system. Grey line in (A) and (B) represents the estimated number of transporters per cell at a continuum of growth rates.

169 not the rate-limiting step of cell division.

170 **Phosphorus and Sulfur Transport**

171 We now turn our attention towards other essential elements, namely phosphorus and sulfur.
 172 Phosphorus is critical to the cellular energy economy in the form of high-energy phosphodiester
 173 bonds making up DNA, RNA, and the NTP energy pool as well as playing a critical role in the post-
 174 translational modification of proteins and defining the polar-heads of lipids. In total, phosphorus
 175 makes up $\approx 3\%$ of the cellular dry mass which in typical experimental conditions is in the form of
 176 inorganic phosphate. The cell membrane has remarkably low permeability to this highly-charged
 177 and critical molecule, therefore requiring the expression of active transport systems. In *E. coli*, the
 178 proton electrochemical gradient across the inner membrane is leveraged to transport inorganic
 179 phosphate into the cell (*Rosenberg et al., 1977*). Proton-solute symporters are widespread in *E.*
180 coli (*Ramos and Kaback, 1977; Booth et al., 1979*) and can have rapid transport rates of 50 to 100
181 molecules per second for sugars and other solutes (BNID: 103159; 111777, *Milo et al. (2010)*). As
182 a more extreme example, the proton transporters in the F₁-F₀ ATP synthase, which leverage the
183 proton electrochemical gradient for rotational motion, can shuttle protons across the membrane at
184 a rate of ≈ 1000 per second (BNID: 104890; 103390, (*Milo et al., 2010*)). In *E. coli* the PitA phosphate
185 transport system has been shown to be very tightly coupled with the proton electrochemical
186 gradient with a 1:1 proton:phosphate stoichiometric ratio (*Harris et al., 2001; Feist et al., 2007*).
187 Taking the geometric mean of the aforementioned estimates gives a plausible rate of phosphate
188 transport on the order of 300 per second. Illustrated in *Figure 3(A)*, we can estimate that ≈ 150
189 phosphate transporters are necessary to maintain an $\approx 3\%$ dry mass with a 5000 s division time.
190 This estimate is again satisfied when we examine the observed copy numbers of PitA in proteomic
191 data sets (plot in *Figure 3(A)*). While our estimate is very much in line with the observed numbers,
192 we emphasize that this is likely a slight overestimate of the number of transporters needed as there
193 are other phosphorous scavenging systems, such as the ATP-dependent phosphate transporter Pst
194 system which we have neglected.

195 Satisfied that there are a sufficient number of phosphate transporters present in the cell, we
 196 now turn to sulfur transport as another potentially rate limiting process. Similar to phosphate,
 197 sulfate is highly-charged and not particularly membrane permeable, requiring active transport.
 198 While there exists a H+/sulfate symporter in *E. coli*, it is in relatively low abundance and is not well
 199 characterized (*Zhang et al., 2014a*). Sulfate is predominantly acquired via the ATP-dependent ABC
 200 transporter CysUWA system which also plays an important role in selenium transport (*Sekowska
 201 et al., 2000; Sirko et al., 1995*). While specific kinetic details of this transport system are not readily
 202 available, generic ATP transport systems in prokaryotes transport on the order of 1 to 10 molecules
 203 per second (BNID: 109035, *Milo et al. (2010)*). Combining this generic transport rate, measurement
 204 of sulfur comprising 1% of dry mass, and a 5000 second division time yields an estimate of \approx
 205 1000 CysUWA complexes per cell (*Figure 3(B)*). Once again, this estimate is in notable agreement
 206 with proteomic data sets, suggesting that there are sufficient transporters present to acquire the
 207 necessary sulfur. In a similar spirit of our estimate of phosphorus transport, we emphasize that
 208 this is likely an overestimate of the number of necessary transporters as we have neglected other
 209 sulfur scavenging systems that are in lower abundance.

210 **Limits on Transporter Expression**

211 So which, if any, of these processes may be rate limiting for growth? As suggested by *Figure 2*
 212 (B), induced expression can lead to an order-of-magnitude (or more) increase in the amount of
 213 transporters needed to facilitate transport. Thus, if acquisition of nutrients was the limiting state
 214 in cell division, could expression simply be increased to accommodate faster growth? A way to
 215 approach this question is to compute the amount of space in the bacterial membrane that could be
 216 occupied by nutrient transporters. Considering a rule-of-thumb for the surface area of *E. coli* of
 217 about 6 μm^2 (BNID: 101792, *Milo et al. (2010)*), we expect an areal density for 1000 transporters to

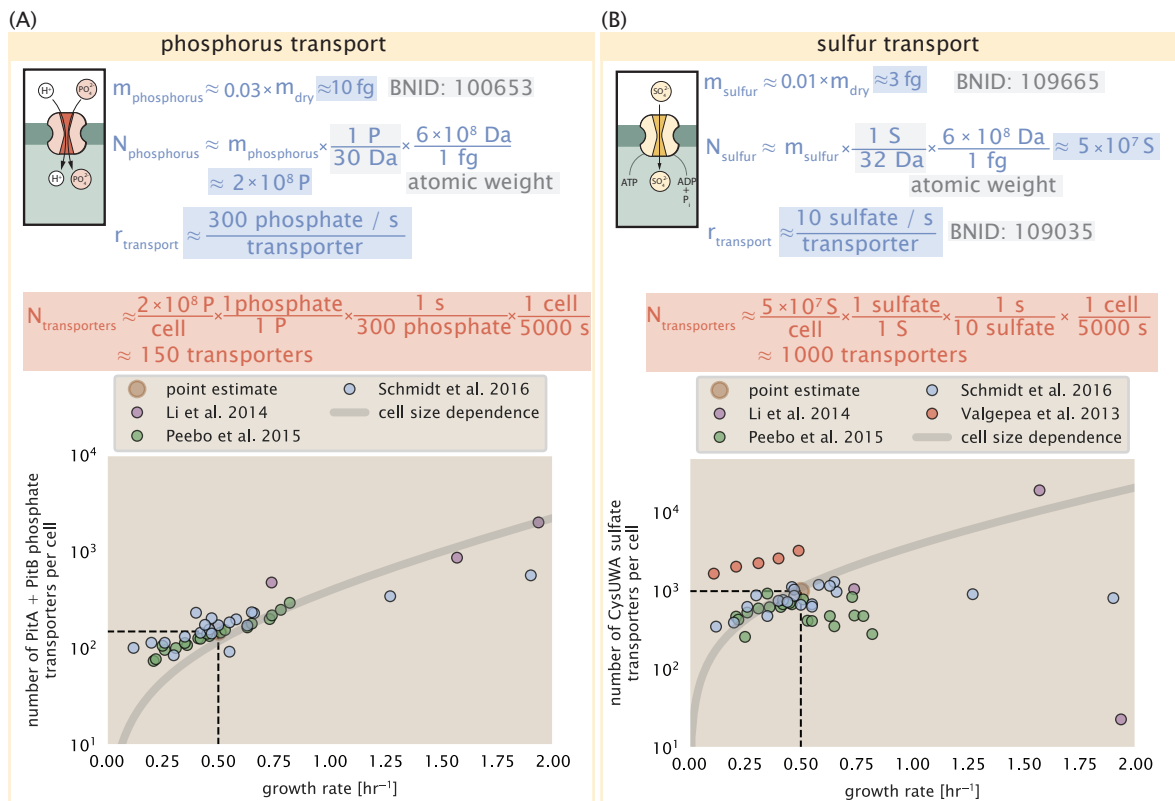


Figure 3. Estimates and measurements of phosphate and sulfate transport systems as a function of growth rate. (A) Estimate for the number of PitA phosphate transport systems needed to maintain a 3% phosphorus *E. coli* dry mass. Points in plot correspond to the total number of PitA transporters per cell. (B) Estimate of the number of CysUWA complexes necessary to maintain a 1% sulfur *E. coli* dry mass. Points in plot correspond to average number of CysUWA transporter complexes that can be formed given the transporter stoichiometry [CysA]₂[CysU][CysW][Sbp/CysP]. Grey line in (A) and (B) represents the estimated number of transporters per cell at a continuum of growth rates.

218 be approximately 200 transporters/ μm^2 . For a typical transporter occupying about 50 nm 2 /dimer,
 219 this amounts to about only 1 percent of the total inner membrane (*Szenk et al., 2017*). In addition,
 220 bacterial cell membranes typically have densities of 10^5 proteins/ μm^2 (*Phillips, 2018*), implying that
 221 the cell could accommodate more transporters of a variety of species if it were rate limiting. As we
 222 will see in the next section, however, occupancy of the membrane can impose other limits on the
 223 rate of energy production.

224 Energy Production

225 While the transport of nutrients is required to build new cell mass, the metabolic pathways both
 226 consume and generate energy in the form of NTPs. The high-energy phosphodiester bonds
 227 of (primarily) ATP power a variety of cellular processes that drive biological systems away from
 228 thermodynamic equilibrium. The next set of processes we hypothesize might control the rate of
 229 cell division considers the energy budget of a dividing cell in terms of the synthesis of ATP from
 230 ADP and inorganic phosphate as well as maintenance of the electrochemical proton gradient which
 231 powers it.

232 ATP Synthesis

233 Hydrolysis of the terminal phosphodiester bond of ATP forming ADP and an inorganic phosphate is
 234 a kinetic driving force in a wide array of biochemical reactions. One such reaction is the formation
 235 of peptide bonds during translation which requires ≈ 2 ATPs for the charging of an amino acid to
 236 the tRNA and ≈ 2 ATP equivalents for the formation of the peptide bond between amino acids.
 237 Considering the ATP costs associated with error correction and post-translational modifications
 238 of proteins, we can make the approximation that each peptide bond has a net cost of ≈ 5 ATP
 239 (BNID: 107782, *Milo et al. (2010)*). In total, the energetic costs of peptide bond formation consume
 240 $\approx 80\%$ of the cells ATP budget (BNID: 107782; 106158; 101637; 111918, *Milo et al. (2010)*; *Lynch*
 241 and *Marinov (2015)*; *Stouthamer (1973)*). The pool of ATP is produced by the F₁-F₀ ATP synthase – a
 242 membrane-bound rotary motor which under ideal conditions can yield ≈ 300 ATP per second (BNID:
 243 114701; *Milo et al. (2010)*; *Weber and Senior (2003)*).

244 To estimate the total number of ATP equivalents consumed during a cell cycle, we will make the
 245 approximation that there are $\approx 3 \times 10^6$ proteins per cell with an average protein length of ≈ 300
 246 peptide bonds (BNID: 115702; 108986; 104877, *Milo et al. (2010)*). Taking these values together,
 247 we estimate that the typical *E. coli* cell consumes $\approx 5 \times 10^9$ ATP per cell cycle on protein synthesis
 248 alone and $\approx 6 \times 10^9$ ATP in total. Assuming that the ATP synthases are operating at their fastest
 249 possible rate, ≈ 3000 ATP synthases are needed to keep up with the energy demands of the cell.
 250 This estimate and a comparison with the data are shown in *Figure 4* (A). Despite our assumption of
 251 maximal ATP production rate per synthase and approximation of all NTP consuming reactions being
 252 the same as ATP, we find that an estimate of a few thousand complete synthases per cell to agree
 253 well with the experimental data. Much as we did for the estimates of transporter copy number in
 254 the previous section, we can generalize this estimation to consider a continuum of growth rates
 255 rather than a point estimate of 5000 s, indicated by the gray lines in *Figure 4*, and find that this
 256 approach adequately describes the observed growth rate dependence.

257 If the direct production of ATP was a rate limiting step for growth, could the cell simply express
 258 more ATP synthase complexes? This requires us to consider several features of cellular physiology,
 259 namely the physical space on the inner membrane as well as the ability to maintain the proton
 260 chemical gradient leveraged by the synthase to drive ATP production out of equilibrium.

261 Generating the Proton Electrochemical Gradient

262 In order to produce ATP, the F₁-F₀ ATP synthase itself must consume energy. Rather than burning
 263 through its own product, this intricate macromolecular machine has evolved to exploit the elec-
 264 trochemical potential established across the inner membrane through cellular respiration. This
 265 electrochemical gradient is manifest by the pumping of protons into the intermembrane space via

266 the electron transport chains as they reduce NADH. In *E. coli*, this potential difference is ≈ -200 mV
 267 (BNID: 102120, *Milo et al. (2010)*). A simple estimate of the inner membrane as a capacitor with a
 268 working voltage of -200 mV (as performed in the Supplemental Information) reveals that $\approx 2 \times 10^4$
 269 protons must be present in the intermembrane space.

270 However, the constant rotation of the ATP synthases would rapidly abolish this potential differ-
 271 ence if it were not being actively maintained. To undergo a complete rotation (and produce a single
 272 ATP), the F₁-F₀ ATP synthase must shuttle ≈ 4 protons across the membrane into the cytosol (BNID:
 273 103390, *Milo et al. (2010)*). With ≈ 3000 ATP synthases each generating 300 ATP per second, the
 274 2×10^4 protons establishing the 200 mV potential would be consumed in only a few milliseconds.
 275 This brings us to our next estimate: how many electron transport complexes are needed to support
 276 the consumption rate of the ATP synthases?

277 The electrochemistry of the electron transport complexes of *E. coli* have been the subject of
 278 intense biochemical and biophysical study over the past half century (*Ingledew and Poole, 1984;*
 279 *Khademian and Imlay, 2017; Cox et al., 1970; Henkel et al., 2014*). A recent work (*Szenk et al.,*
 280 *2017*) examined the respiratory capacity of the *E. coli* electron transport complexes using structural
 281 and biochemical data, revealing that each electron transport chain rapidly pumps protons into
 282 the intermembrane space at a clip of ≈ 1500 protons per second (BIND: 114704; 114687, *Milo*
 283 *et al. (2010)*). Using our estimate of the number of ATP synthases required per cell (*Figure 4(A)*),
 284 coupled with these recent measurements, we estimate that ≈ 1000 electron transport complexes
 285 would be necessary to facilitate the $\approx 4 \times 10^6$ protons per second diet of the cellular ATP synthases.
 286 This estimate (along with a generalization to the entire range of observed growth rates) is in
 287 agreement with the number of complexes identified in the proteomic datasets (plot in *Figure 4(B)*).
 288 This suggests that every ATP synthase must be accompanied by ≈ 1 functional electron transport
 289 chain. Again, if this were a rate limiting process for bacterial growth, one must conclude that it is
 290 not possible for the cell to simply increase the production of both the number of electron transport
 291 chain complexes as well as ATP synthases. As both of these components only function bound to
 292 the inner membrane, we now turn our attention towards the available space in the membrane as
 293 well as surface-area-to-volume constraints.

294 Energy Production in a Crowded Membrane.

295 For each protein considered so far, the data shows that in general their numbers increase with
 296 growth rate. This is in part a consequence of the increase in cell length and width at that is common
 297 to many rod-shaped bacteria at faster growth rates (*Ojikic et al., 2019; Harris and Theriot, 2018*).
 298 For the particular case of *E. coli*, the total cellular protein and cell size increase logarithmically
 299 with growth rate (*Schaechter et al., 1958; Si et al., 2017*). Indeed, this is one reason why we have
 300 considered only a single, common growth condition across all our estimates so far. Such a scaling
 301 will require that the total number of proteins and net demand on resources also grow in proportion
 302 to the increase in cell size divided by the cell's doubling time. Recall however that each transport
 303 process, as well as the ATP production via respiration, is performed at the bacterial membrane. This
 304 means that their maximum productivity can only increase in proportion to the cell's surface area
 305 divided by the cell doubling time. This difference in scaling would vary in proportion to the surface
 306 area-to-volume (S/V) ratio.

307 While we found that there was more than sufficient membrane real estate for carbon intake in
 308 our earlier estimate, the total number of ATP synthases and electron chain transport complexes
 309 both exhibit a clear increase in copy number with growth rate, reaching in excess of 10^4 copies per
 310 cell (*Figure 4*). Here we consider the consequences of this S/V ratio scaling in more detail.

311 In our estimate of ATP production above we found that a cell demands about 6×10^9 ATP or
 312 10^6 ATP/s. With a cell volume of roughly 1 fL, this corresponds to about 2×10^{10} ATP per fL of cell
 313 volume, in line with previous estimates (*Stouthamer and Bettenhausen, 1977; Szenk et al., 2017*).
 314 In *Figure 5* (A) we plot this ATP demand as a function of the S/V ratio in green, where we have
 315 considered a range of cell shapes from spherical to rod-shaped with an aspect ratio (length/width)

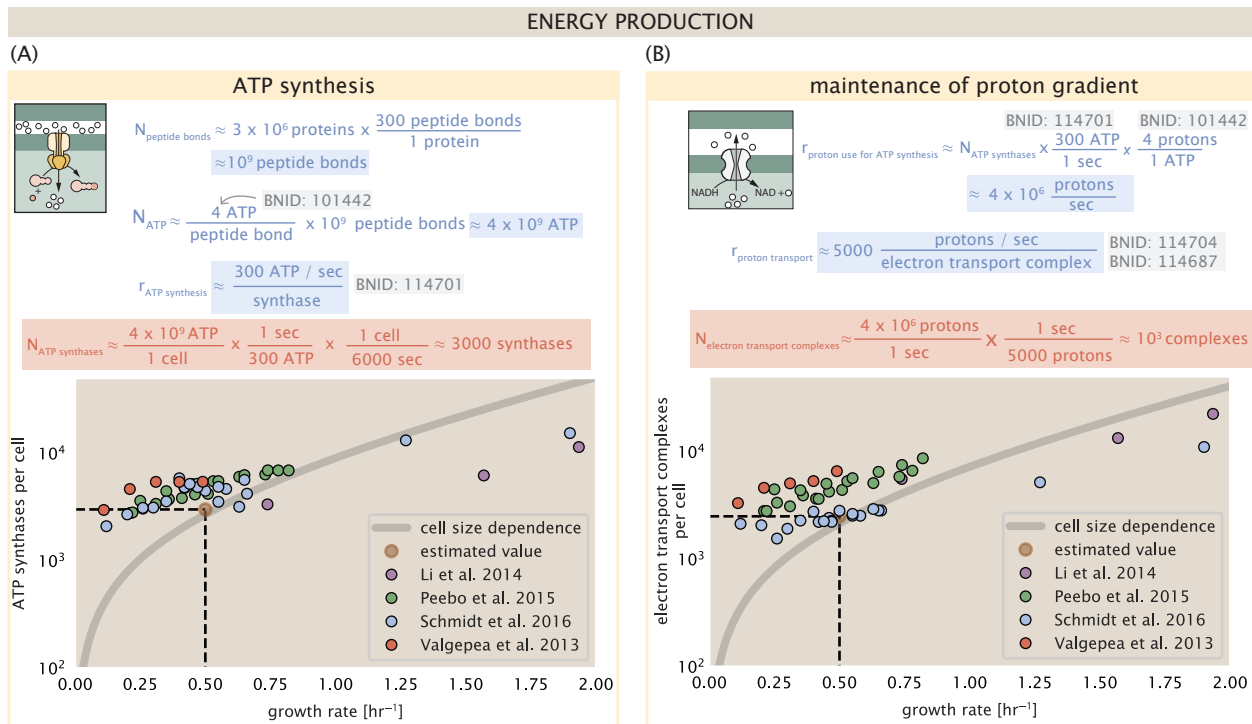


Figure 4. The abundance of F₁-F₀ ATP synthases and electron transport chain complexes as a function of growth rate. (A) Estimate of the number of F₁-F₀ ATP synthase complexes needed to accommodate peptide bond formation and other NTP dependent processes. Points in plot correspond to the mean number of complete F₁-F₀ ATP synthase complexes that can be formed given proteomic measurements and the subunit stoichiometry [AtpE]₁₀[AtpF]₂[AtpB][AtpC][AtpH][AtpA]₃[AtpG][AtpD]₃. (B) Estimate of the number of electron transport chain complexes needed to maintain a membrane potential of ~ -200 mV given estimate of number of F₁-F₀ ATP synthases from (A). Points in plot correspond to the average number of complexes identified as being involved in aerobic respiration by the Gene Ontology identifier GO:0019646 that could be formed given proteomic observations. These complexes include cytochromes *bd1* ([CydA][CydB][CydX][CydH]), *bdII* ([AppC][AppB]), *bo3*, ([CyoD][CyoA][CyoB][CyoC]) and NADH:quinone oxidoreductase I ([NuoA][NuoH][NuoJ][NuoK][NuoL][NuoM][NuoN][NuoB][NuoC][NuoE][NuoF][NuoG][NuoI]) and II ([Ndh]). Grey lines in both (A) and (B) correspond to the estimate procedure described, but applied to a continuum of growth rates. We direct the reader to the Supporting Information for a more thorough description of this approach.

316 equal to 4 (See appendix for calculations of cell volume and surface area). In order to consider the
 317 maximum power that could be produced, we consider the amount of ATP that can be generated by a
 318 membrane filled with ATP synthase and electron transport complexes, which provides a maximal
 319 production of about 3 ATP / (nm²·s) (*Szenk et al., 2017*). This is shown in blue in **Figure 5(A)**, which
 320 shows that at least for the growth rates observed, the energy demand is roughly an order of
 321 magnitude less.

322 Interestingly, *Szenk et al. (2017)* also found that ATP production by respiration is less efficient
 323 than by fermentation per membrane area occupied due to the additional proteins of the electron
 324 transport chain. This suggests that even under anaerobic growth, there will be sufficient membrane
 325 space for ATP production in general.

326 While this serves to highlight the diminishing capacity to provide resources to grow if the cell
 327 increases in size (and its S/V decreases), the blue region in **Figure 5(A)** represents a somewhat
 328 unachievable limit since the inner membrane must also include other proteins such as those
 329 required for lipid and membrane synthesis. To gain insight, we used the proteomic data to look at
 330 the distribution of proteins on the inner membrane. Here we use Gene Ontology (GO) annotations
 331 (*Ashburner et al., 2000; The Gene Ontology Consortium, 2018*) to identify all proteins embedded or
 332 peripheral to the inner membrane (GO term: 0005886). Those associated but not membrane-bound
 333 include proteins like MreB and FtsZ, that traverse the inner membrane by treadmilling and must
 334 nonetheless be considered as a vital component occupying space on the membrane. In **Figure 5(B)**,
 335 we find that the total protein mass per μm² is relatively constant with growth rate. Interestingly,
 336 when we consider the distribution of proteins grouped by their Clusters of Orthologous Groups
 337 (COG) (*Tatusov et al., 2000*), the relative abundance for those in metabolism (including ATP synthesis
 338 via respiration) is also relatively constant.

339 **Function of the Central Dogma**

340 Up to this point, we have considered a variety of transport and biosynthetic processes that are
 341 critical to acquiring and generating new cell mass. While there are of course many other metabolic
 342 processes we could consider and perform estimates of (such as the components of fermentative
 343 versus aerobic respiration), we now turn our focus to some of the most central processes which
 344 *must* be undertaken irrespective of the growth conditions – the processes of the central dogma.

345 **DNA**

346 Most bacteria (including *E. coli*) harbor a single, circular chromosome and can have extra-chromosomal
 347 plasmids up to ~ 100 kbp in length. We will focus our quantitative thinking solely on the chromo-
 348 some of *E. coli* which harbors ≈ 5000 genes and ≈ 5 × 10⁶ base pairs. To successfully divide and
 349 produce viable progeny, this chromosome must be faithfully replicated and segregated into each
 350 nascent cell. We again rely on the near century of literature in molecular biology to provide some
 351 insight on the rates and mechanics of the replicative feat as well as the production of the required
 352 starting materials, dNTPs.

353 **dNTP synthesis**

354 We begin our exploration DNA replication by examining the production of the deoxyribonucleotide
 355 triphosphates (dNTPs). The four major dNTPs (dATP, dTTP, dCTP, and dGTP) are synthesized *de novo*
 356 in separate pathways, requiring different building blocks. However, a critical step present in all
 357 dNTP synthesis pathways is the conversion from ribonucleotide to deoxyribonucleotide via the
 358 removal of the 3' hydroxyl group of the ribose ring (*Rudd et al., 2016*). This reaction is mediated by a
 359 class of enzymes termed ribonucleotide reductases, of which *E. coli* possesses two aerobically active
 360 complexes (termed I and II) and a single anaerobically active enzyme. Due to their peculiar formation
 361 of a radical intermediate, these enzymes have received much biochemical, kinetic, and structural
 362 characterization. One such work (*Ge et al., 2003*) performed a detailed *in vitro* measurement of the
 363 steady-state kinetic rates of these complexes, revealing a turnover rate of ≈ 10 dNTP per second.

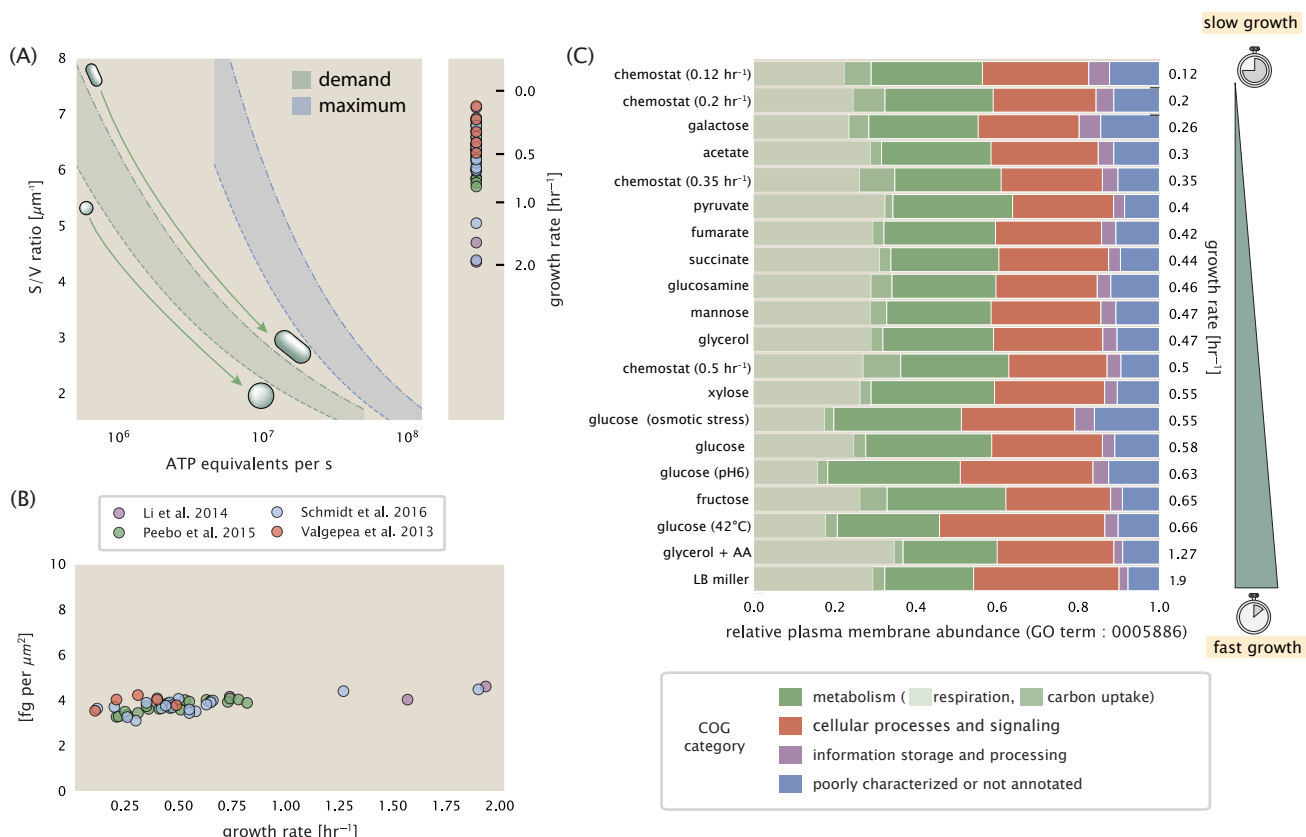


Figure 5. Influence of cell size and S/V ratio on ATP production and inner membrane composition. (A) Scaling of ATP demand and maximum ATP production as a function of S/V ratio. Cell volumes of 0.5 fL to 50 fL were considered, with the dashed (—) line corresponding to a sphere and the dash-dot line (---) reflecting a rod-shaped bacterium like *E. coli* with a typical aspect ratio (length / width) of 0.4 (Shi et al., 2018). Approximately 50% of the bacterial inner membrane is assumed to be protein, with the remainder lipid. (B) Total protein mass calculated for proteins with inner membrane annotation (GO term: 0005886). (C) Relative protein abundances by mass based on COG annotation. Metabolic proteins are further separated into respiration (F_1 - F_0 ATP synthase, NADH dehydrogenase I, succinate:quinone oxidoreductase, cytochrome b o₃ ubiquinol oxidase, cytochrome bd-I ubiquinol oxidase) and carbohydrate transport (GO term: GO:0008643). Note that the elongation factor EF-Tu can also associate with the inner membrane, but was excluded in this analysis due to its high relative abundance (roughly identical to the total mass shown in part (B)).

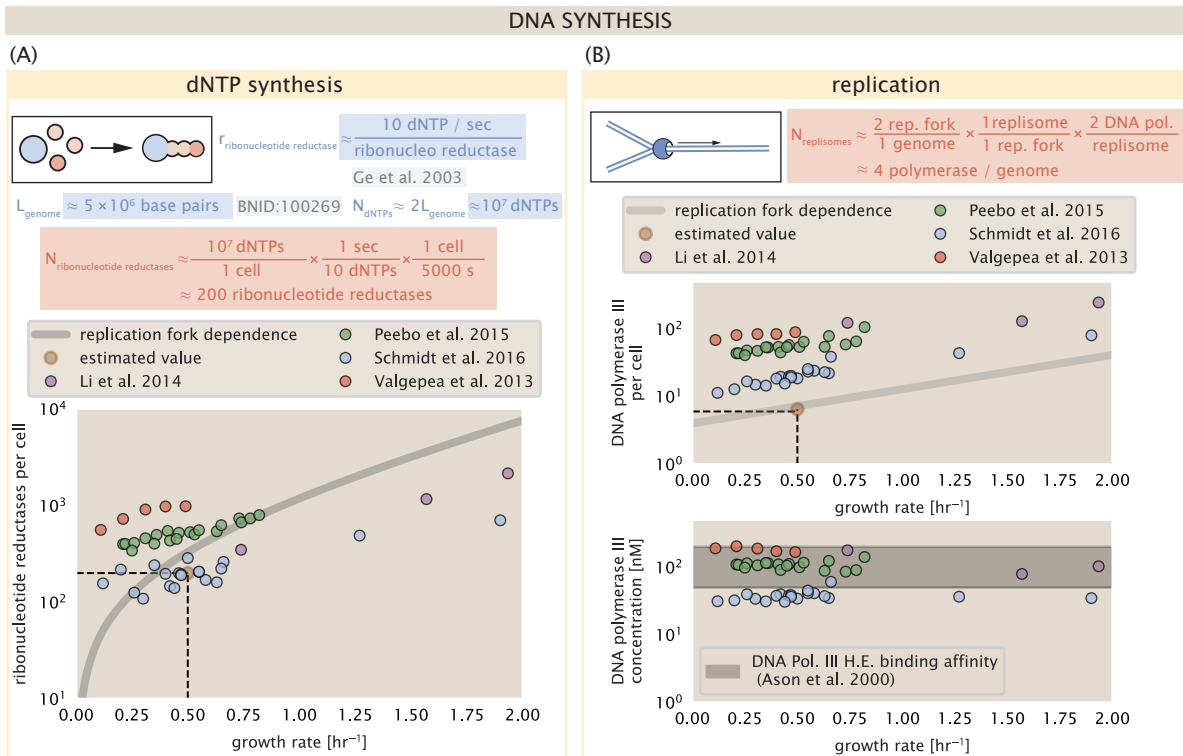


Figure 6. Complex abundance estimates for dNTP synthesis and DNA replication. (A) Estimate of the number of ribonucleotide reductase enzymes needed to facilitate the synthesis of $\approx 10^7$ dNTPs over the course of a 5000 second generation time. Points in the plot correspond to the total number of ribonucleotide reductase I ($[NrdA]_2[NrdB]_2$) and ribonucleotide reductase II ($[NrdE]_2[NrdF]_2$) complexes. (B) An estimate for the minimum number of DNA polymerase holoenzyme complexes needed to facilitate replication of a single genome. Points in the top plot correspond to the total number of DNA polymerase III holoenzyme complexes ($[DnaE]_3[DnaQ]_3[HolE]_3[DnaX]_5[HolB][HolA][DnaN]_4[HolC]_4[HolD]_4$) per cell. Bottom plot shows the effective concentration of DNA polymerase III holoenzyme given cell volumes calculated from the growth rate as in *Sj et al. (2019)* (See Supplemental Information Section 4). Grey lines in (A) and top panel of (B) show the estimated number of complexes needed as a function of growth, the details of which are described in the Supplemental Information.

364 Since this reaction is central to the synthesis of all dNTPs, it is reasonable to consider the
 365 abundance of these complexes is a measure of the total dNTP production in *E. coli*. Illustrated
 366 schematically in **Figure 6** (A), we consider the fact that to replicate the cell's genome, on the order of
 367 $\approx 10^7$ dNTPs must be synthesized. Assuming a production rate of 10 per second per ribonucleotide
 368 reductase complex and a cell division time of 5000 seconds, we arrive at an estimate of ≈ 200
 369 complexes needed per cell. As shown in the bottom panel of **Figure 6** (A), this estimate agrees
 370 with the experimental measurements of these complexes abundances within $\approx 1/2$ an order of
 371 magnitude. Extension of this estimate across a continuum of growth rate, including the fact that
 372 multiple chromosomes can be replicated at a given time, is shown as a grey transparent line in
 373 **Figure 6** (A). Similarly to our point estimate, this refinement agrees well with the data, accurately
 374 describing both the magnitude of the complex abundance and the dependence on growth rate.

375 Recent work has revealed that during replication, the ribonucleotide reductase complexes
 376 coalesce to form discrete foci colocalized with the DNA replisome complex (*Sánchez-Romero et al.*,
 377 **2011**). This is particularly pronounced in conditions where growth is slow, indicating that spatial
 378 organization and regulation of the activity of the complexes plays an important role.

379 DNA Replication

380 We now turn our focus to the integration of these dNTP building blocks into the replicated chromo-
 381 some strand via the DNA polymerase. Replication is initiated at a single region of the chromosome
 382 termed the *oriC* locus at which a pair of DNA polymerases bind and begin their high-fidelity replica-

383 tion of the genome in opposite directions. Assuming equivalence between the two replication forks,
 384 this means that the two DNA polymerase complexes (termed replisomes) meet at the midway point
 385 of the circular chromosome termed the *ter* locus. The kinetics of the five types of DNA polymerases
 386 (I – V) have been intensely studied, revealing that DNA polymerase III performs the high fidelity
 387 processive replication of the genome with the other "accessory" polymerases playing auxiliary roles
 388 (*Fjalkowska et al., 2012*). *In vitro* measurements have shown that DNA Polymerase III copies DNA
 389 at a rate of \approx 600 nucleotides per second (BNID: 104120, *Milo et al. (2010)*). Therefore, to replicate
 390 a single chromosome, two replisomes (containing two DNA polymerase III each) moving at their
 391 maximal rate would copy the entire genome in \approx 4000 s. Thus, with a division time of 5000 s (our
 392 "typical" growth rate for the purposes of this work), there is sufficient time for a pair of replisomes
 393 complexes to replicate the entire genome. However, this estimate implies that 4000 s would be the
 394 upper-limit time scale for bacterial division which is at odds with the familiar 20 minute (1200 s)
 395 doubling time of *E. coli* in rich medium.

396 It is well known that *E. coli* can parallelize its DNA replication such that multiple chromosomes
 397 are being replicated at once, with as many as 10 - 12 replication forks at a given time (*Bremer*
 398 and *Dennis, 2008*; *Si et al., 2017*). Thus, even in rapidly growing cultures, we expect only a few
 399 polymerases (\approx 10) are needed to replicate the chromosome per cell doubling. However, as shown
 400 in **Figure 6(B)**, DNA polymerase III is nearly an order of magnitude more abundant. This
 401 discrepancy can be understood by considering its binding constant to DNA. DNA polymerase III
 402 is highly processive, facilitated by a strong affinity of the complex to the DNA. *In vitro* biochemical
 403 characterization has quantified the K_D of DNA polymerase III holoenzyme to single-stranded and
 404 double-stranded DNA to be 50 and 200 nM, respectively (*Ason et al., 2000*). The bottom plot in
 405 **Figure 6** (B) shows that the concentration of the DNA polymerase III across all data sets and growth
 406 conditions is within this range. Thus, while the copy number of the DNA polymerase III is in excess
 407 of the strict number required to replicate the genome, its copy number appears to vary such that its
 408 concentration is approximately equal to the dissociation constant to the DNA. While the processes
 409 regulating the initiation of DNA replication are complex and involve more than just the holoenzyme,
 410 these data indicate that the kinetics of replication rather than the explicit copy number of the DNA
 411 polymerase III holoenzyme is the more relevant feature of DNA replication to consider. In light
 412 of this, the data in **Figure 6(B)** suggests that for bacteria like *E. coli*, DNA replication does not represent a rate-limiting step in cell division. However, it is worth noting that for bacterium like *C. crescentus* whose chromosomal replication is initiated only once per cell cycle (*Jensen et al., 2001*), the time to double their chromosome likely represents an upper limit to their growth rate.

416 RNA Synthesis

417 With the machinery governing the replication of the genome accounted for, we now turn our
 418 attention to the next stage of the central dogma – the transcription of DNA to form RNA. We
 419 primarily consider three major groupings of RNA, namely the RNA associated with ribosomes
 420 (rRNA), the RNA encoding the amino-acid sequence of proteins (mRNA), and the RNA which links
 421 codon sequence to amino-acid identity during translation (tRNA). Despite the varied function of
 422 these RNA species, they share a commonality in that they are transcribed from DNA via the action
 423 of RNA polymerase. In the coming paragraphs, we will consider the synthesis of RNA as a rate
 424 limiting step in bacterial division by estimating how many RNA polymerases must be present to
 425 synthesize all necessary rRNA, mRNA, and tRNA.

426 rRNA

427 We begin with an estimation of the number of RNA polymerases needed to synthesize the rRNA
 428 that serve as catalytic and structural elements of the ribosome. Each ribosome contains three rRNA
 429 molecules of lengths 120, 1542, and 2904 nucleotides (BNID: 108093, *Milo et al. (2010)*), meaning
 430 each ribosome contains \approx 4500 nucleotides. As the *E. coli* RNA polymerase transcribes DNA to RNA
 431 at a rate of \approx 40 nucleotides per second (BNID: 101904, *Milo et al. (2010)*), it takes a single RNA

432 polymerase \approx 100 s to synthesize the RNA needed to form a single functional ribosome. Therefore,
 433 in a 5000 s division time, a single RNA polymerase transcribing rRNA at a time would result in only
 434 \approx 50 functional ribosomal rRNA units – far below the observed number of $\approx 10^4$ ribosomes per cell.

435 Of course, there can be more than one RNA polymerase transcribing the rRNA genes at any
 436 given time. To elucidate the *maximum* number of rRNA units that can be synthesized given a single
 437 copy of each rRNA gene, we will consider a hypothesis in which the rRNA operon is completely tiled
 438 with RNA polymerase. *In vivo* measurements of the kinetics of rRNA transcription have revealed that
 439 RNA polymerases are loaded onto the promoter of an rRNA gene at a rate of \approx 1 per second (BNID:
 440 111997; 102362, *Milo et al. (2010)*). If RNA polymerases are being constantly loaded on to the rRNA
 441 genes at this rate, then we can assume that \approx 1 functional rRNA unit is synthesized per second.
 442 With a 5000 second division time, this hypothesis leads to a maximal value of 5000 functional rRNA
 443 units, still undershooting the observed number of 10^4 ribosomes per cell.

444 *E. coli*, like many other bacterium, have evolved a clever mechanism to surpass this kinetic limit
 445 for the rate of rRNA production. Rather than having only one copy of each rRNA gene, *E. coli* has
 446 seven copies of the operon (BIND: 100352, *Milo et al. (2010)*) four of which are localized directly
 447 adjacent to the origin of replication (*Birnbaum and Kaplan, 1971*). As fast growth also implies an
 448 increased gene dosage due to parallelized chromosomal replication, the total number of rRNA
 449 genes can be on the order of \approx 10 – 70 copies at moderate to fast growth rates (*Stevenson and*
 450 *Schmidt, 2004*). Using our standard time scale of a 5000 second division time, we can make the
 451 lower-bound estimate that the typical cell will have 7 copies of the rRNA operon. Synthesizing one
 452 functional rRNA unit per second per rRNA operon, a total of 4×10^4 rRNA units can be synthesized,
 453 comfortably above the observed number of ribosomes per cell.

454 How many RNA polymerases are then needed to constantly transcribe 7 copies of the rRNA
 455 genes? We approach this estimate by considering the maximum number of RNA polymerases tiled
 456 along the rRNA genes with a loading rate of 1 per second and a transcription rate of 40 nucleotides
 457 per second. Considering that a RNA polymerase has a physical footprint of approximately 40
 458 nucleotides (BNID: 107873, *Milo et al. (2010)*), we can expect \approx 1 RNA polymerase per 80 nucleotides.
 459 With a total length of \approx 4500 nucleotides per operon and 7 operons per cell, the maximum number
 460 of RNA polymerases that can be transcribing rRNA at any given time is \approx 400. As we will see in the
 461 coming sections, the synthesis of rRNA is the dominant requirement of the RNA polymerase pool.

462 mRNA

463 To form a functional protein, all protein coding genes must first be transcribed from DNA to form
 464 an mRNA molecule. While each protein requires an mRNA blueprint, many copies of the protein
 465 can be synthesized from a single mRNA. Factors such as strength of the ribosomal binding site,
 466 mRNA stability, and rare codon usage frequency dictate the number of proteins that can be made
 467 from a single mRNA, with yields ranging from 10^1 to 10^4 (BNID: 104186; 100196; 106254, *Milo et al.*
 468 *(2010)*). Computing the geometric mean of this range yields \approx 1000 proteins synthesized per mRNA,
 469 a value that agrees with experimental measurements of the number of proteins per cell ($\approx 3 \times 10^6$,
 470 BNID: 100088, *Milo et al. (2010)*) and total number of mRNA per cell ($\approx 3 \times 10^3$, BNID: 100064, *Milo*
 471 *et al. (2010)*).

472 This estimation captures the *steady-state* mRNA copy number, meaning that at any given time,
 473 there will exist approximately 3000 unique mRNA molecules. To determine the *total* number of
 474 mRNA that need to be synthesized over the cell's lifetime, we must consider degradation of the
 475 mRNA. In most bacteria, mRNAs are rather unstable with life times on the order of several minutes
 476 (BNID: 104324; 106253; 111927; 111998, *Milo et al. (2010)*). For convenience, we assume that the
 477 typical mRNA in our cell of interest has a typical lifetime of \approx 300 seconds. Using this value, we
 478 can determine the total mRNA production rate to maintain a steady-state copy number of 3000
 479 mRNA per cell. While we direct the reader to the appendix for a more detailed discussion of mRNA
 480 transcriptional dynamics, we state here that the total mRNA production rate must be on the order
 481 of \approx 15 mRNA per second. In *E. coli*, the average protein is \approx 300 amino acids in length (BNID:

482 108986; *Milo et al. (2010)*), meaning that the corresponding mRNA is \approx 900 nucleotides which we
 483 will further approximate as \approx 1000 nucleotides to account for the non-protein coding regions on
 484 the 5' and 3' ends. This means that the cell must have enough RNA polymerase molecules about
 485 to sustain a transcription rate of $\approx 1.5 \times 10^4$ nucleotides per second. Knowing that a single RNA
 486 polymerase polymerizes RNA at a clip of 40 nucleotides per second, we arrive at a comfortable
 487 estimate of \approx 250 RNA polymerase complexes needed to satisfy the mRNA demands of the cell. It is
 488 worth noting that this number is approximately half of that required to synthesize enough rRNA, as
 489 we saw in the previous section. We find this to be a striking result as these 250 RNA polymerase
 490 molecules are responsible for the transcription of the \approx 4000 protein coding genes that are not
 491 ribosome associated.

492 tRNA

493 The final class of RNA molecules worthy of quantitative consideration are the tRNAs that are used
 494 during translation to map codon sequence on mRNA to specific amino acids. Unlike mRNA or rRNA,
 495 each individual tRNA is remarkably short, ranging from 70 to 95 nucleotides each (BNID: 109645;
 496 102340, *Milo et al. (2010)*). What they lack in length, they make up for in abundance, with reported
 497 values ranging from $\approx 6 \times 10^4$ (BNID: 105280, *Milo et al. (2010)*) to $\approx 4 \times 10^5$ (BNID: 108611). To test
 498 tRNA synthesis as a possible growth-rate limiting stage, we will err towards a higher abundance of
 499 $\approx 4 \times 10^5$ per cell. Combining the abundance and tRNA length measurements, we make the estimate
 500 that $\approx 5 \times 10^7$ nucleotides are sequestered in tRNA per cell. Unlike mRNA, tRNA is remarkably stable
 501 with typical lifetimes *in vivo* on the order of \approx 48 hours (*Abelson et al., 1974; Svennengsen et al., 2017*) – well beyond the timescale of division. Once again using our rule-of-thumb for the rate of
 502 transcription to be 40 nucleotides per second and assuming a division time of \approx 5000 seconds, we
 503 arrive at an estimate of \approx 150 RNA polymerases to synthesize enough tRNA. This requirement pales
 504 in comparison to the number of polymerases needed to generate the rRNA and mRNA pools and
 505 can be neglected as a significant transcriptional burden.

507 RNA Polymerase and σ -factor Abundance

508 These estimates, summarized in *Figure 7* (A), reveal that synthesis of rRNA and mRNA are the dominant
 509 RNA species synthesized by RNA polymerase, suggesting the need for \approx 700 RNA polymerases
 510 per cell. As is revealed in *Figure 7* (B), this estimate is about an order of magnitude below the observed
 511 number of RNA polymerase complexes per cell (\approx 5000 - 7000). The disagreement between
 512 the estimated number of RNA polymerases and these observations are at least consistent with
 513 recent literature revealing that \approx 80 % of RNA polymerases in *E. coli* are not transcriptionally active
 514 (*Patrick et al., 2015*). Our estimate ignores the possibility that some fraction is only nonspecifically
 515 bound to DNA, as well as the obstacles that RNA polymerase and DNA polymerase present for each
 516 other as they move along the DNA (*Finkelstein and Greene, 2013*).

517 In addition, it is also vital to consider the role of σ -factors which help RNA polymerase identify
 518 and bind to transcriptional start sites (*Browning and Busby, 2016*). Here we consider σ^{70} (RpoD)
 519 which is the dominant "general-purpose" σ -factor in *E. coli*. While initially thought of as being solely
 520 involved in transcriptional initiation, the past two decades of single-molecule work has revealed
 521 a more multipurpose role for σ^{70} including facilitating transcriptional elongation (*Kapanidis et al., 2005; Goldman et al., 2015; Perdue and Roberts, 2011; Mooney and Landick, 2003; Mooney et al., 2005*). *Figure 7* (B) is suggestive of such a role as the number of σ^{70} proteins per cell is in close
 523 agreement with our estimate of the number of transcriptional complexes needed.

525 These estimates provide insight as to the observed magnitude of both RNA polymerase and
 526 the σ -70 factor. As we have done in the previous sections, and described in the supplemental
 527 information, we can generalize these estimates across a wide range of growth rates (grey line in
 528 *Figure 7*(B). While there remains some disagreement in the magnitude of the copy number, this
 529 estimate appears to very adequately describe the growth rate dependence of these complexes.
 530 Furthermore, these findings illustrate that transcription cannot be the rate limiting step in bacterial

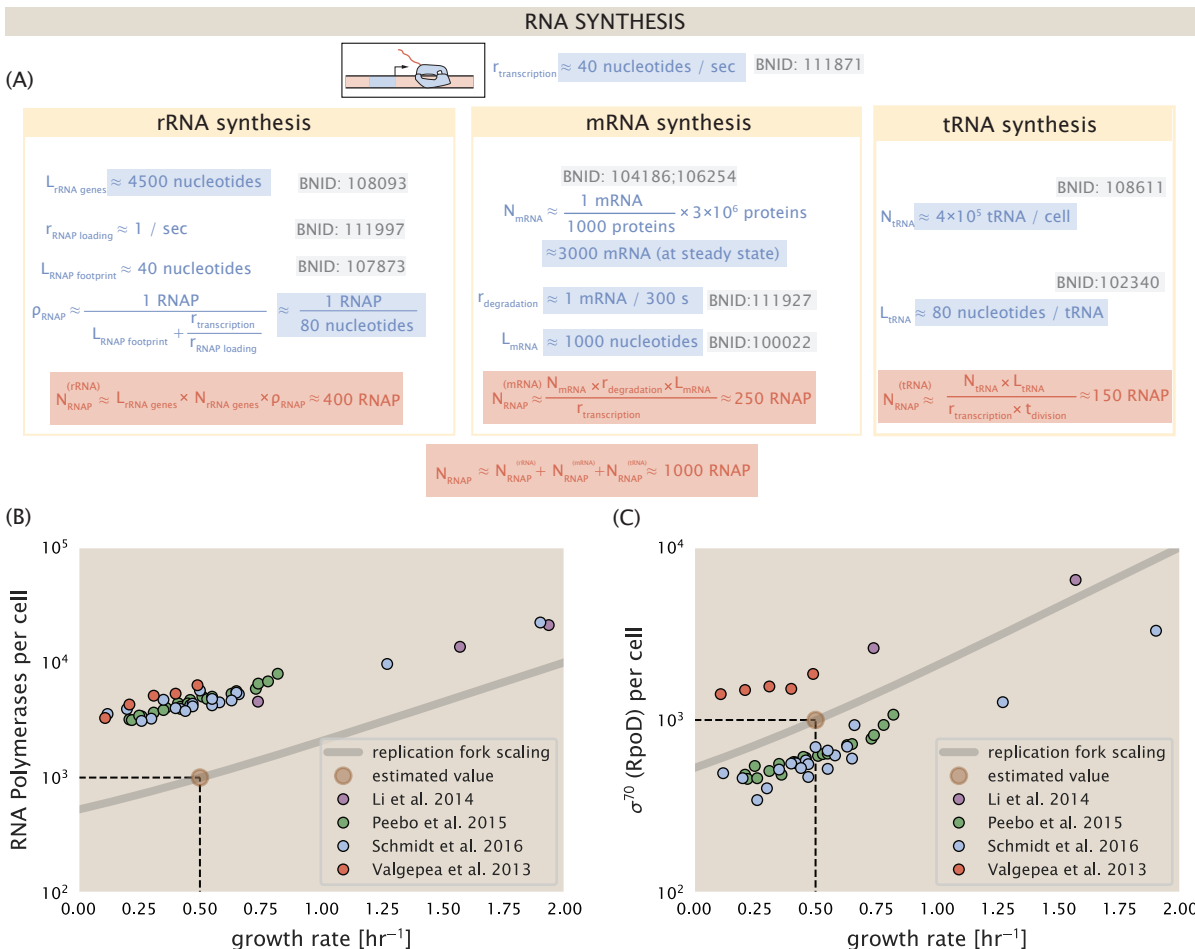


Figure 7. Estimation of the RNA polymerase demand and comparison with experimental data. (A) Estimations for the number of RNA polymerase needed to synthesize sufficient quantities of rRNA, mRNA, and tRNA from left to right, respectively. Bionumber Identifiers (BNIDs) are provided for key quantities used in the estimates. (B) The RNA polymerase core enzyme copy number as a function of growth rate. Colored points correspond to the average number RNA polymerase core enzymes that could be formed given a subunit stoichiometry of $[RpoA]_2[RpoC][RpoB]$. (C) The abundance of σ^{70} as a function of growth rate. Estimated value for the number of RNAP is shown in (B) and (C) as a translucent brown point at a growth rate of 0.5 hr^{-1} .

division. **Figure 7** (A) reveals that the availability of RNA polymerase is not a limiting factor for cell division as the cell always has an apparent ~ 10-fold excess than needed. Furthermore, if more transcriptional activity was needed to satisfy the cellular requirements, more σ^{70} -factors could be expressed to utilize a larger fraction of the RNA polymerase pool.

535 Translation and Ribosomal Synthesis

536 Lastly, we turn our attention to the process of synthesizing new proteins, translation. This process
 537 stands as a good candidate for potentially limiting growth since the synthesis of new proteins relies
 538 on the generation of ribosomes, themselves proteinaceous molecules. As we will see in the coming
 539 sections of this work, this poses a "chicken-or-the-egg" problem where the synthesis of ribosomes
 540 requires ribosomes in the first place.

541 We will begin our exploration of protein translation in the same spirit as we have in previous
 542 sections – we will draw order-of-magnitude estimates based on our intuition and available literature,
 543 and then compare these estimates to the observed data. In doing so, we will estimate both the
 544 absolute number of ribosomes necessary for replication of the proteome as well as the synthesis
 545 of amino-acyl tRNAs. From there we consider the limitations on ribosomal synthesis in light of our
 546 estimates on both the synthesis of ribosomal proteins and our earlier results on rRNA synthesis.

547 tRNA Synthetases

548 We begin by first estimating the number of tRNA synthetases in *E. coli* needed to convert free
 549 amino-acids to polypeptide chains. At a doubling time of ≈ 5000 s, *E. coli* has roughly 3×10^6 proteins
 550 per cell (BNID: 115702; *Milo et al. (2010)*). Assuming that the typical protein is on the order of ≈ 300
 551 amino acids in length (BNID: 100017; *Milo et al. (2010)*), we can estimate that a total of $\approx 10^9$ amino
 552 acids are stitched together by peptide bonds.

553 How many tRNAs are needed to facilitate this remarkable number of amino acid delivery events
 554 to the translating ribosomes? It is important to note that tRNAs are recycled after they've passed
 555 through the ribosome and can be recharged with a new amino acid, ready for another round
 556 of peptide bond formation. While some *in vitro* data exists on the turnover of tRNA in *E. coli* for
 557 different amino acids, we can make a reasonable estimate by comparing the number of amino
 558 acids to be polymerized to cell division time. Using our stopwatch of 5000 s and 10^9 amino acids, we
 559 arrive at a requirement of $\approx 2 \times 10^5$ tRNA molecules to be consumed by the ribosome per second.

560 There are many processes which go into synthesizing a tRNA and ligating it with the appropriate
 561 amino acids. As we discussed previously, there appear to be more than enough RNA polymerases
 562 per cell to synthesize the needed pool of tRNAs. Without considering the many ways in which
 563 amino acids can be scavenged or synthesized *de novo*, we can explore ligation the as a potential
 564 rate limiting step. The enzymes which link the correct amino acid to the tRNA, known as tRNA
 565 synthetases or tRNA ligases, are incredible in their proofreading of substrates with the incorrect
 566 amino acid being ligated once out of every 10^4 to 10^5 times (BNID: 103469, *Milo et al. (2010)*). This is
 567 due in part to the consumption of energy as well as a multi-step pathway to ligation. While the rate
 568 at which tRNA is ligated is highly dependent on the identity of the amino acid, it is reasonable to
 569 state that the typical tRNA synthetase has charging rate of ≈ 20 AA per tRNA synthetase per second
 570 (BNID: 105279, *Milo et al. (2010)*).

571 We can make an assumption that amino-acyl tRNAs are in steady-state where they are produced
 572 at the same rate they are consumed, meaning that 2×10^5 tRNAs must be charged per second.
 573 Combining these estimates together, as shown schematically in **Figure 8(A)**, yields an estimate of
 574 $\approx 10^4$ tRNA synthetases per cell with a division time of 5000 s. This point estimate is in very close
 575 agreement with the observed number of synthetases (the sum of all 20 tRNA synthetases in *E. coli*).
 576 This estimation strategy seems to adequately describe the observed growth rate dependence of
 577 the tRNA synthetase copy number (shown as the grey line in **Figure 8(B)**), suggesting that the copy
 578 number scales with the cell volume.

579 In total, the estimated and observed $\approx 10^4$ tRNA synthetases occupy only a meager fraction of

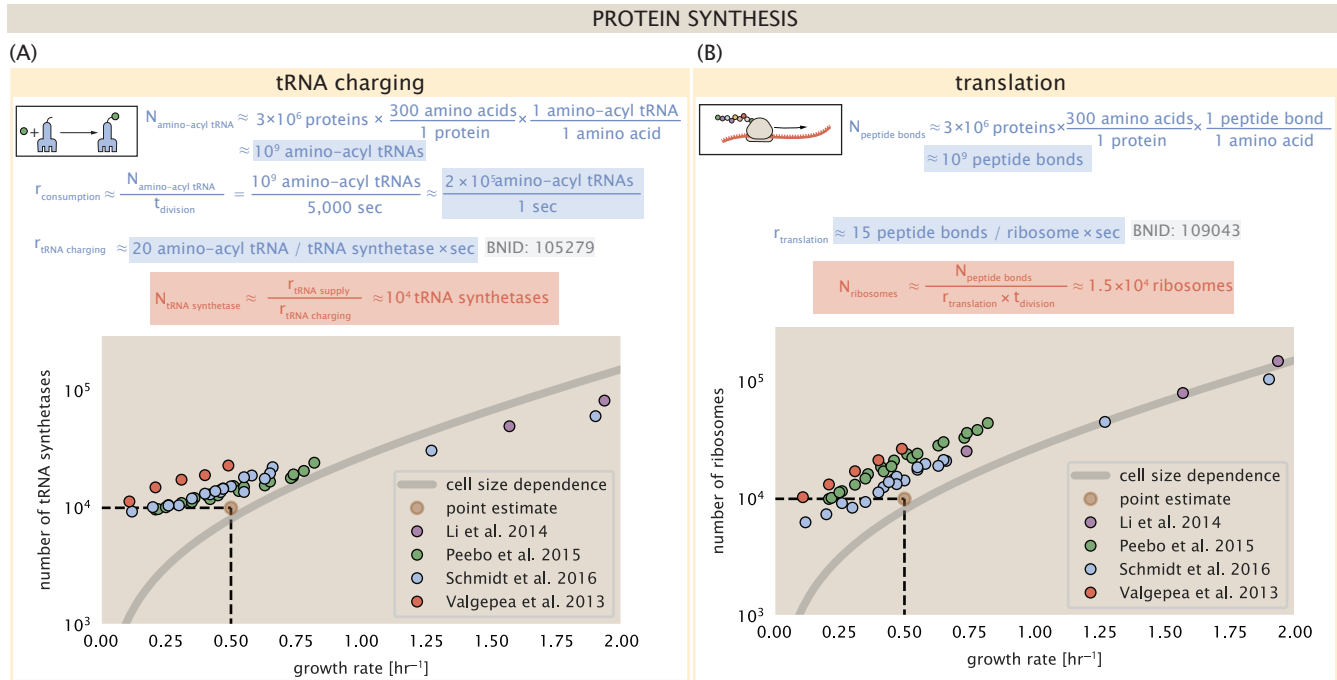


Figure 8. Estimation of the required tRNA synthetases and ribosomes. (A) Estimation for the number of tRNA synthetases that will supply the required amino acid demand. The sum of all tRNA synthetases copy numbers are plotted as a function of growth rate ([ArgS], [CysS], [GlnS], [GltX], [IleS], [LeuS], [ValS], [AlaS]₂, [AsnS]₂, [AspS]₂, [TyrS]₂, [TrpS]₂, [ThrS]₂, [SerS]₂, [ProS]₂, [PheS]₂[PheT]₂, [MetG]₂, [lysS]₂, [HisS]₂, [GlyS]₂[GlyQ]₂). (B) Estimation of the average abundance of ribosomes required to synthesize 10⁹ peptide bonds with an elongation rate of 15 peptide bonds per second. Our estimated values are shown for a growth rate of 0.5 hr⁻¹. Grey lines correspond to the estimated complex abundance calculated at different growth rates. See Supplemental Information XX for a more detail description of this calculation.

the total cell proteome, around 0.5% by abundance. It is reasonable to assume that if tRNA charging was a rate limiting process, cells would be able to increase their growth rate by devoting more cellular resources to making more tRNA synthetases. As the synthesis of tRNAs and the corresponding charging can be highly parallelized, we can argue that tRNA charging is not a rate limiting step in cell division, at least for the growth conditions explored in this work.

585 Protein Synthesis

With the number of tRNA synthetases accounted for, we now consider the abundance of the protein synthesis machines themselves, ribosomes. Ribosomes are enormous protein/rRNA complexes that facilitate the peptide bond formation between amino acids in the correct sequence as defined by the coding mRNA. Before we examine the synthesis of the ribosome proteins and the limits that may place on the observed bacterial growth rates, let's consider replication of the cellular proteome.

As described in the previous section, an *E. coli* cell consisting of $\approx 3 \times 10^6$ proteins will have on the order $\approx 10^9$ peptide bonds per proteome. While the rate at which ribosomes translates is well known to have a growth rate dependence *Dai et al. (2018)* and is a topic which we discuss in detail in the coming sections. However, for the purposes of our order-of-magnitude estimate, we can make the approximation that translation occurs at a rate of ≈ 15 amino acids per second per ribosome (BNID: 100233, *Milo et al. (2010)*). Under this approximation and assuming a division time of 5000 s, we can arrive at an estimate of $\approx 10^4$ ribosomes are needed to replicate the cellular proteome, shown in *Figure 8(B)*. This point estimate, while glossing over important details such as chromosome copy number and growth-rate dependent translation rates, proves to be notably accurate when compared to the experimental observations (*Figure 8(B)*).

601 **Translation and Ribosomal Synthesis as a Growth-Rate Limiting Step**

602 Thus far, the general back-of-the-envelope estimates have been reasonably successful in explaining
 603 what sets the scale of absolute protein copy number. A recurring theme that has arisen is the ability
 604 of cells to parallelize their biosynthesis tasks. For example, while DNA replication speed-limit is
 605 ≈ 40 minutes to replicate a genome, cells can divide faster than this by initiating more than one
 606 round of replication per doubling. The process of protein synthesis overall doesn't appear to be
 607 rate-limiting, since for example, cells are able to induce the expression of additional enzymes to
 608 grow on alternative carbon sources. However, as we will see, the synthesis of ribosomal proteins
 609 presents a special case where parallelization is not possible (*Figure 9(A)*). Thus, it is plausible that
 610 translation may be a key factor in determining the cellular growth rate.

611 To gain some intuition into how translation can set the speed of bacterial growth, we again
 612 consider the total number of peptide bonds that must be synthesized, which we denote as N_{AA} .
 613 With cells growing exponentially in time (*Godin et al., 2010*), we can compute the number of amino
 614 acids to be polymerized as

$$N_{AA}\lambda = r_t R, \quad (1)$$

615 where λ is the cell growth rate in s^{-1} , r_t is the maximum translation rate in $AA \cdot s^{-1}$, and R is the
 616 average ribosome copy number per cell. Knowing the number of peptide bonds to be formed
 617 permits us to compute the translation-limited growth rate as

$$\lambda_{\text{translation-limited}} = \frac{r_t R}{N_{AA}}. \quad (2)$$

618 Alternatively, since N_{AA} is related to the total protein mass through the molecular weight of
 619 each protein, we can also consider the growth rate in terms of the fraction of the total proteome
 620 mass dedicated to ribosomal proteins. By making the approximation that an average amino acid
 621 has a molecular weight of 110 Da (BNID: 104877, *Milo et al. (2010)*), the total protein mass m_{protein} is
 622 related to N_{AA} by $(m_{\text{protein}}/110 \text{ Da}) \times N_A$, where N_A is Avogadro's number. Similarly, R is related to
 623 the ribosomal protein mass by $R \approx (m_R/800 \text{ Da}) \times N_A$, where 800 Da reflects the summed molecular
 624 weight of all ribosomal subunits. This allows us to approximate $R/N_{AA} \approx \Phi_R/L_R$, where Φ_R is
 625 the ribosomal mass fraction m_{protein}/m_R , and L_R the ratio of 800 kDa / 110 Da per amino acid or,
 626 alternatively, the total length in amino acids that make up a ribosome. The translation-limited
 627 growth rate can then be written in the form

$$\lambda_{\text{translation-limited}} \approx \frac{r_t}{L_R} \Phi_R. \quad (3)$$

628 This is plotted as a function of ribosomal fraction Φ_R in *Figure 9(B)*, where we take $L_R = 7459$ AA,
 629 corresponding to the length in amino acids for all ribosomal subunits of the 50S and 30S complex
 630 (BNID: 101175, *Milo et al., 2010*).

631 The growth rate defined by *Equation 3* reflects mass-balance under steady-state growth and
 632 has long provided a rationalization of the apparent linear increase in *E. coli*'s ribosomal content
 633 as a function of growth rate (*Maaløe, 1979; Scott et al., 2010*). Here we see that there will be a
 634 maximum rate when $\Phi_R = 1$, which for a translation rate of 17 amino acids per second, gives us
 635 $\lambda \approx 8 \text{ hr}^{-1}$, or a doubling time just under 6 minutes (*Figure 9(B)*, dashed line). Interestingly, this limit
 636 is independent of the absolute number of ribosomes and is simply given by the time to translate
 637 an entire ribosome, L_R/r_t . As shown in *Figure 9(A)*, we can reconcile this with the observation
 638 that in order to double the average number of ribosomes, each ribosome must produce a second
 639 ribosome and this process cannot be parallelized. Unless protein synthesis can increase, or cells
 640 can trim their total ribosomal protein mass, this must represent an absolute speed limit for cell
 641 doubling.

642 Earlier, we considered rRNA synthesis (see Section **RNA Synthesis**), finding that, when the rRNA
 643 operons are maximally loaded with RNA polymerase, the cell can produce ≈ 1 functional rRNA
 644 unit per second per operon. In *Figure 9(C)*, we show the maximum number of ribosomes that

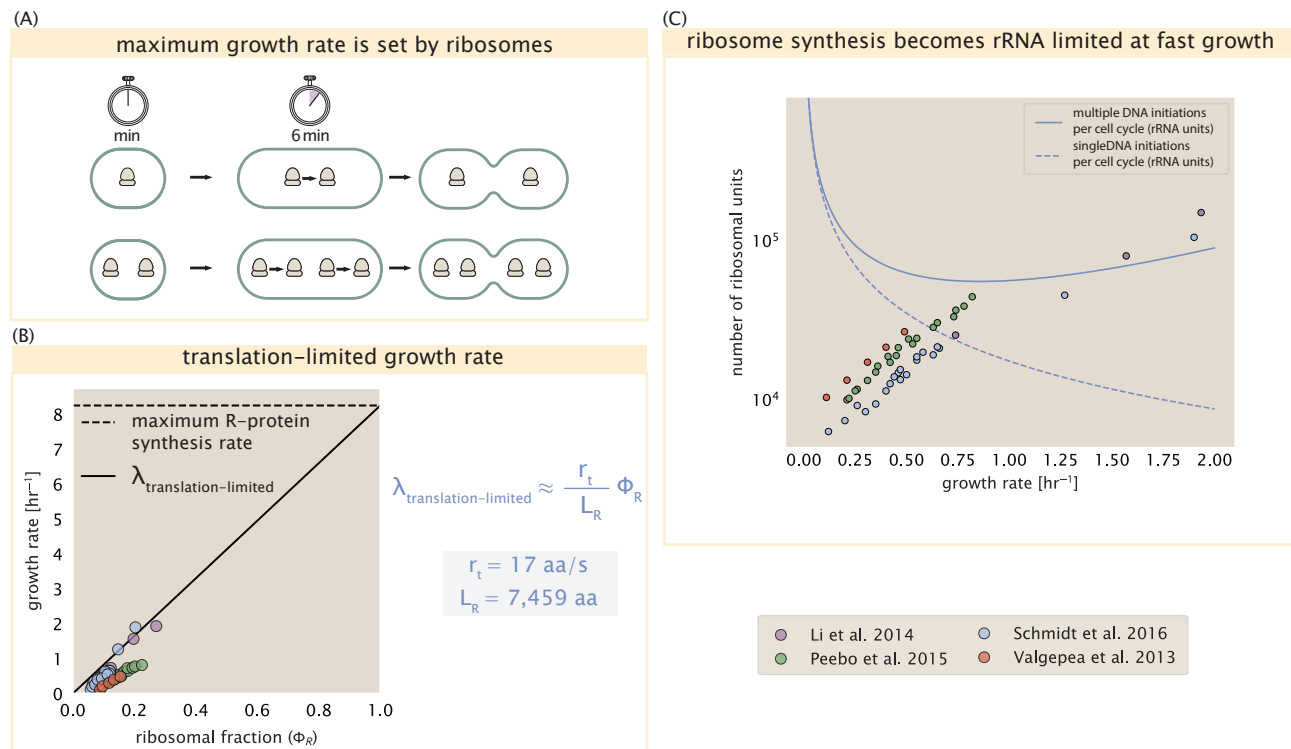


Figure 9. Translation-limited growth rate. (A) An inherent maximum growth rate is set by the time to synthesize all ribosomal subunits. This growth rate is given by r_t/L_R , where r_t is the elongation rate and L_R is the total number of amino acids that make up the entire ribosomal complex. This rate is independent of the number of ribosomes; instead limited serial requirement for each ribosome to double itself. (B) Here we consider the translation-limited growth as a function of ribosomal fraction, as defined in Equation 3. The solid line is calculated for an elongation rate of 17 aa per second. The dashed line corresponds to the maximum rate of ribosomal protein (R-protein) synthesis considered in part (A). [inset needed to show smaller region where data is.] (C) Maximum number of rRNA units that can be synthesized as a function of growth rate. Solid curve corresponds to the rRNA copy number is calculated by multiplying the number of rRNA operons by the estimated number of (# ori) at each growth rate. The quantity (# ori) was calculated using Equation 4 and the measurements from *Si et al. (2017)* that are plotted in Figure 10(A). The dashed line shows the maximal number of functional rRNA units produced from a single chromosomal initiation per cell cycle.

could be made as a function of growth rate given this rRNA production rule-of-thumb. While each *E. coli* genome has 7 copies of the rRNA operon (BNID: 107866, *Milo et al. (2010)*), parallelization of DNA synthesis by firing multiple rounds of replication at a time can drastically increase the effective number of rRNA operons. The blue curve in *Figure 9(C)*, we assume that the effective number of rRNA operons increases in proportion to the number of origins of replication $\langle \# \text{ ori} \rangle$ (solid blue line; with the calculation of $\langle \# \text{ ori} \rangle$ described in the next section). Although we expect this value to drastically overestimate rRNA abundance at slower growth rates ($\lambda < 0.5 \text{ hr}^{-1}$), it provides a useful reference when considered along with the proteomic measurements that are also plotted. For growth rates above about 1 hr^{-1} , we find that cells will need to transcribe rRNA near their maximal rate. The dashed blue curve in *Figure 9(C)* shows the maximal number of functional rRNA units that could be synthesized from a single genome (ignoring the chromosome replication speed limit of ≈ 40 minutes per genome). The convergence between the maximum rRNA production with parallelization and the experimentally measured ribosome copy number (points in *Figure 9(C)*), suggests rRNA synthesis may begin to present a bottleneck in cell division at the fastest growth rates. While this strain of *E. coli* is rarely reported to grow faster than 2 hr^{-1} , other bacteria with more copies of rRNA genes have been found that surpass this growth rate (*Bremer and Dennis, 2008; Roller et al., 2016*).

Relationship Between Cell Size and Growth Rate

The relationship between cell size and growth rate has long been of interest in the study of bacterial physiology, particularly following the now six decade-old observation that cell volume appears to increase exponentially with growth rate; known as Schaechter's growth law (*Schaechter et al., 1958; Taheri-Araghi et al., 2015*). However, the mechanism that governs this relationship, and even the question of whether the change in average cell size is truly exponential has remained under debate (*Harris and Theriot, 2018*). Given the important of cell size in determining the total protein mass that must be doubled, and in setting other parameters like the surface-area-to-volume ratio, in this final section we leverage our proteomic data to consider cell size and growth rate.

In *Figure 9(B)* we found that at moderate growth rates (above about 0.5 hr^{-1}), cells are growing at a rate near maximum given their ribosomal fraction Φ_R . This means that in order to grow any faster, cells must increase Φ_R further. A naïve strategy following the constraint of *Equation 3* is simply that cells should make additional ribosomes. In reality, however, large swaths of the proteome increase in absolute protein abundance as cells grow faster (Supplemental Figure X), and the ability to add additional ribosomes is likely constrained by other factors including crowding due to their large size (*Delarue et al., 2018; Soler-Bistué et al., 2020*). Instead, it is well-documented that *E. coli* cells add a constant volume per origin of replication, which is robust to a remarkable array of cellular perturbations (*Si et al., 2017*). To consider this in the context of the proteomic data, we used the measurements from *Si et al. (2017)* for wild-type *E. coli* cells grown in different nutrient conditions (*Figure 10(A)*) to estimate the average number of origins per cell $\langle \# \text{ ori} \rangle$ across the data. Indeed, we find an approximately linear trend between protein copy number and $\langle \# \text{ ori} \rangle$, and in *Figure 10(B)* plot this for ribosomal copy numbers.

The average number of origins $\langle \# \text{ ori} \rangle$ is set by how often replication must be initiated per cell doubling under steady-state growth, and can be quantified via

$$\langle \# \text{ ori} \rangle = 2^{t_{\text{cyc}}/\tau} = 2^{t_{\text{cyc}}\lambda/\ln(2)}, \quad (4)$$

where t_{cyc} is the cell cycle time (referring to the time from replication initiation to cell division), and τ is the cell doubling time. For a constant cell cycle time, observed at growth rates above about 0.5 hr^{-1} (*Helmstetter and Cooper, 1968*), *Equation 4* says that $\langle \# \text{ ori} \rangle$ will increase exponentially with the growth rate.

Insight into why cells add a constant volume per $\langle \# \text{ ori} \rangle$, and how this relates to growth, however, requires us to consider the changes in the proteome, and in particular ribosomal proteins across the different growth conditions. In *Figure 10(D)* we consider the position-dependent protein expression

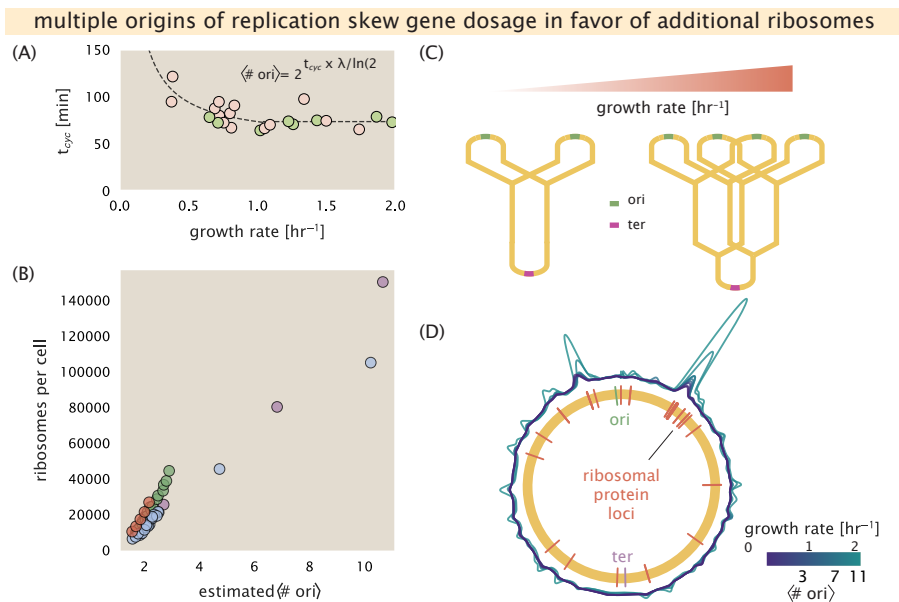


Figure 10. Multiple replication initiations bias protein synthesis in favor of more ribosomes. (A) Experimental data from Si *et al.* (2017). Dashed line shows fit to the data, which were used to estimate $\langle \# \text{ori} \rangle$. t_{cyc} was assumed to vary in proportion to τ for doubling times great than 40 minutes, and then reach a minimum value of [fill in] minutes below this (see Supplemental Appendix X for additional details). Red data points correspond to measurements in strain MG1655, while light green points are for strain NCM3722. (B) Plot of the ribosome copy number estimated from the proteomic data against the estimated $\langle \# \text{ori} \rangle$. (C) Schematic shows the expected increase in replication forks (or number of ori regions) as *E. coli* cells grow faster. (D) A running Gaussian average (20 kbp st. dev.) of protein copy number is calculated for each growth condition considered by (Schmidt *et al.*, 2016). Since total protein abundance increases with growth rate, protein copy numbers are median-subtracted to allow comparison between growth conditions. $\langle \# \text{ori} \rangle$ are estimated using the data in (A) and Equation 4. [still looking into how best to use this type of analysis]

693 across the chromosome for each of the growth conditions from Schmidt *et al.* (2016). Here we
 694 calculated a running Gaussian average of protein copy number (20 kbp st. dev. averaging window)
 695 based on each gene's transcriptional start site, which were then median-subtracted to account for
 696 the differences in total protein abundance with each growth condition. Importantly, we find that
 697 the major deviations in protein copy number are largely restricted to regions of ribosomal protein
 698 genes, with substantially higher deviations observed for cells with high $\langle \# \text{ori} \rangle$ (teal), as compared
 699 to those with low $\langle \# \text{ori} \rangle$ (purple). This is particularly apparent for genes closer to the origin, where
 700 the majority of ribosomal proteins are found. This suggests that in addition to the linear scaling
 701 between protein abundance and $\langle \# \text{ori} \rangle$, cells are also varying their relative ribosomal abundance
 702 in proportion to $\langle \# \text{ori} \rangle$. Since growth rate depends specifically on the ribosomal fraction Φ_R , this
 703 result suggests that cells are changing their size as a way to tune Φ_R to match the available nutrient
 704 conditions.

705 While this dependence between cell size and ribosomal abundance is apparent across moderate
 706 to fast growth rates, it is worth noting that this scaling is likely to change at slow growth rates
 707 (below $\lambda \approx 0.5 \text{ hr}^{-1}$). Here, the number of ribosomes R no longer reflects the cell's protein synthesis
 708 capacity (Dai *et al.*, 2016), so far taken to be $r_i \times R$, and instead, cells have an excess number of
 709 ribosomes. Additional regulatory control through the small-molecule alarmones such as guanosine
 710 pentaphosphate [(p)ppGpp] reduce the fraction of actively translating ribosomes at these slower
 711 growth rates. This overabundance of ribosomes provides different challenges on the ability of the
 712 cell to maintain steady-state growth under limiting nutrient conditions, and in Supplemental Section
 713 XX we consider this slow growth regime further.

714 As a final comment, it has recently been shown that growth in a (p)ppGpp null strain also lacked
 715 both the condition-dependent changes in $\langle \# \text{ori} \rangle$ as well as changes in cell size across different
 716 growth condition. Instead, cells always exhibited a high ratio of $\langle \# \text{ori} \rangle$ to $\langle \# \text{ter} \rangle$, irrespective of

717 growth rate, and a cell size that was more consistent with a fast growth state where (p)ppGpp levels
718 are normally low (*Fernández-Coll et al., 2020*) and ribosomal fraction is high (*Zhu and Dai, 2019*).
719 There is also evidence that this may be achieved through inhibition of DNA replication initiation
720 (*Kraemer et al., 2019*). These observations raise the possibility that (p)ppGpp may be playing a
721 causal role in tuning $\langle \# \text{ ori} \rangle$ and cell size, which ultimately allows the cell to vary its ribosomal
722 content according to nutrient availability.

723 [This last paragraph may be better placed in the discussion]

724 References

- 725 **Abelson HT**, Johnson LF, Penman S, Green H. Changes in RNA in Relation to Growth of the Fibroblast: II.
726 The Lifetime of mRNA, rRNA, and tRNA in Resting and Growing Cells. *Cell*. 1974 Apr; 1(4):161–165. doi:
727 10.1016/0092-8674(74)90107-X.
- 728 **Aideland G**, Towbin BD, Rothschild D, Dekel E, Bren A, Alon U. Hierarchy of Non-Glucose Sugars in *Escherichia*
729 *coli*. *BMC Systems Biology*. 2014 Dec; 8(1):133. doi: 10.1186/s12918-014-0133-z.
- 730 **Antonenko YN**, Pohl P, Denisov GA. Permeation of Ammonia across Bilayer Lipid Membranes Studied by
731 Ammonium Ion Selective Microelectrodes. *Biophysical Journal*. 1997 May; 72(5):2187–2195.
- 732 **Ashburner M**, Ball CA, Blake JA, Botstein D, Butler H, Cherry JM, Davis AP, Dolinski K, Dwight SS, Eppig JT, Harris
733 MA, Hill DP, Issel-Tarver L, Kasarskis A, Lewis S, Matese JC, Richardson JE, Ringwald M, Rubin GM, Sherlock G.
734 Gene Ontology: tool for the unification of biology. *Nature Genetics*. 2000 May; 25(1):25–29.
- 735 **Ason B**, Bertram JG, Hingorani MM, Beechem JM, O'Donnell M, Goodman MF, Bloom LB. A Model for *Escherichia*
736 *coli* DNA Polymerase III Holoenzyme Assembly at Primer/Template Ends: DNA Triggers A Change In Binding
737 Specificity of the γ Complex Clamp Loader. *Journal of Biological Chemistry*. 2000 Jan; 275(4):3006–3015. doi:
738 10.1074/jbc.275.4.3006.
- 739 **Assentoft M**, Kaptan S, Schneider HP, Deitmer JW, de Groot BL, MacAulay N. Aquaporin 4 as a NH₃ Channel.
740 *Journal of Biological Chemistry*. 2016 Sep; 291(36):19184–19195. doi: 10.1074/jbc.M116.740217.
- 741 **Bauer S**, Ziv E. Dense Growth of Aerobic Bacteria in a Bench-Scale Fermentor. *Biotechnology and Bioengineering*. 1976; 18(1):81–94. doi: 10.1002/bit.260180107, _eprint:
742 https://onlinelibrary.wiley.com/doi/pdf/10.1002/bit.260180107.
- 743 **Belliveau NM**, Barnes SL, Ireland WT, Jones DL, Sweredoski MJ, Moradian A, Hess S, Kinney JB, Phillips R. Systematic Approach for Dissecting the Molecular Mechanisms of Transcriptional Regulation in Bacteria. *Proceedings of the National Academy of Sciences*. 2018 May; 115(21):E4796–E4805. doi: 10.1073/pnas.1722055115.
- 744 **Birnbaum LS**, Kaplan S. Localization of a Portion of the Ribosomal RNA Genes in *Escherichia coli*. *Proceedings of the National Academy of Sciences*. 1971 May; 68(5):925–929. doi: 10.1073/pnas.68.5.925.
- 745 **Booth IR**, Mitchell WJ, Hamilton WA. Quantitative Analysis of Proton-Linked Transport Systems. The Lactose
746 Permease of *Escherichia coli*. *Biochemical Journal*. 1979 Sep; 182(3):687–696.
- 747 **Bremer H**, Dennis PP. Modulation of Chemical Composition and Other Parameters of the Cell at Different
748 Exponential Growth Rates. *EcoSal Plus*. 2008 Oct; 3(1).
- 749 **Browning DF**, Busby SJW. Local and global regulation of transcription initiation in bacteria. *Nature Reviews
750 Microbiology*. 2016 Aug; 14(10):638–650.
- 751 **Cox GB**, Newton NA, Gibson F, Snoswell AM, Hamilton JA. The Function of Ubiquinone in *Escherichia coli*.
752 *Biochemical Journal*. 1970 Apr; 117(3):551–562. doi: 10.1042/bj1170551.
- 753 **Dai X**, Zhu M, Warren M, Balakrishnan R, Okano H, Williamson JR, Fredrick K, Hwa T. Slowdown of Translational
754 Elongation in *Escherichia coli* under Hyperosmotic Stress. - PubMed - NCBI. *mBio*. 2018 Feb; 9(1):281.
- 755 **Dai X**, Zhu M, Warren M, Balakrishnan R, Patsalo V, Okano H, Williamson JR, Fredrick K, Wang YP, Hwa T. Reduction
756 of translating ribosomes enables *Escherichia coli* to maintain elongation rates during slow growth. *Nature
757 Microbiology*. 2016 Dec; 2(2):16231.
- 758 **Delarue M**, Brittingham GP, Pfeffer S, Surovtsev IV, Pinglay S, Kennedy KJ, Schaffer M, Gutierrez JL, Sang D,
759 Poterewicz G, Chung JK, Plitzko JM, Groves JT, Jacobs-Wagner C, Engel BD, Holt LJ. mTORC1 Controls Phase
760 Separation and the Biophysical Properties of the Cytoplasm by Tuning Crowding. *Cell*. 2018 Jul; 174(2):338–
761 349.e20.
- 762 **Escalante A**, Salinas Cervantes A, Gosset G, Bolívar F. Current Knowledge of the *Escherichia coli* Phosphoenolpyru-
763 vate–Carbohydrate Phototransferase System: Peculiarities of Regulation and Impact on Growth and Prod-
764 uct Formation. *Applied Microbiology and Biotechnology*. 2012 Jun; 94(6):1483–1494. doi: 10.1007/s00253-
765 012-4101-5.
- 766 **Feist AM**, Henry CS, Reed JL, Krummenacker M, Joyce AR, Karp PD, Broadbelt LJ, Hatzimanikatis V, Palsson BØ. A
767 Genome-Scale Metabolic Reconstruction for *Escherichia coli* K-12 MG1655 That Accounts for 1260 ORFs and
768 Thermodynamic Information. *Molecular Systems Biology*. 2007 Jan; 3(1):121. doi: 10.1038/msb4100155.

- 773 **Fernández-Coll L**, Maciąg-Dorszynska M, Tailor K, Vadia S, Levin PA, Szalewska-Palasz A, Cashel M, Dunny GM.
 774 The Absence of (p)ppGpp Renders Initiation of *Escherichia coli* Chromosomal DNA Synthesis Independent of
 775 Growth Rates. *mBio*. 2020 Apr; 11(2):45.
- 776 **Fijalkowska IJ**, Schaaper RM, Jonczyk P. DNA Replication Fidelity in *Escherichia coli*: A Multi-DNA Polymerase
 777 Affair. *FEMS Microbiology Reviews*. 2012 Nov; 36(6):1105–1121. doi: [10.1111/j.1574-6976.2012.00338.x](https://doi.org/10.1111/j.1574-6976.2012.00338.x).
- 778 **Finkelstein IJ**, Greene EC. Molecular Traffic Jams on DNA. *Annual Review of Biophysics*. 2013 May; 42(1):241–263.
- 779 **Gama-Castro S**, Salgado H, Santos-Zavaleta A, Ledezma-Tejeida D, Muñiz-Rascado L, García-Sotelo JS, Alquicira-
 780 Hernández K, Martínez-Flores I, Pannier L, Castro-Mondragón JA, Medina-Rivera A, Solano-Lira H, Bonavides-
 781 Martínez C, Pérez-Rueda E, Alquicira-Hernández S, Porrón-Sotelo L, López-Fuentes A, Hernández-Koutoucheva
 782 A, Moral-Chávez VD, Rinaldi F, et al. RegulonDB Version 9.0: High-Level Integration of Gene Regulation,
 783 Coexpression, Motif Clustering and Beyond. *Nucleic Acids Research*. 2016 Jan; 44(D1):D133–D143. doi:
 784 10.1093/nar/gkv1156.
- 785 **Ge J**, Yu G, Ator MA, Stubbe J. Pre-Steady-State and Steady-State Kinetic Analysis of *E. coli* Class I Ribonucleotide
 786 Reductase. *Biochemistry*. 2003 Sep; 42(34):10071–10083. doi: [10.1021/bi034374r](https://doi.org/10.1021/bi034374r).
- 787 **Godin M**, Delgado FF, Son S, Grover WH, Bryan AK, Tzur A, Jorgensen P, Payer K, Grossman AD, Kirschner
 788 MW, Manalis SR. Using buoyant mass to measure the growth of single cells. *Nature Methods*. 2010 Apr;
 789 7(5):387–390.
- 790 **Goldman SR**, Nair NU, Wells CD, Nickels BE, Hochschild A. The Primary σ Factor in *Escherichia coli* Can Access the
 791 Transcription Elongation Complex from Solution *In Vivo*. *eLife*. 2015 Sep; 4:e10514. doi: [10.7554/eLife.10514](https://doi.org/10.7554/eLife.10514).
- 792 **Harris LK**, Theriot JA. Surface Area to Volume Ratio: A Natural Variable for Bacterial Morphogenesis. *Trends in
 793 microbiology*. 2018 Oct; 26(10):815–832.
- 794 **Harris RM**, Webb DC, Howitt SM, Cox GB. Characterization of PitA and PitB from *Escherichia coli*. *Journal of
 795 Bacteriology*. 2001 Sep; 183(17):5008–5014. doi: [10.1128/JB.183.17.5008-5014.2001](https://doi.org/10.1128/JB.183.17.5008-5014.2001).
- 796 **van Heeswijk WC**, Westerhoff HV, Boogerd FC. Nitrogen Assimilation in *Escherichia coli*: Putting Molecular
 797 Data into a Systems Perspective. *Microbiology and Molecular Biology Reviews*. 2013 Dec; 77(4):628–695. doi:
 798 [10.1128/MMBR.00025-13](https://doi.org/10.1128/MMBR.00025-13).
- 799 **Heldal M**, Norland S, Tumyr O. X-Ray Microanalytic Method for Measurement of Dry Matter and Elemental
 800 Content of Individual Bacteria. *Applied and Environmental Microbiology*. 1985 Nov; 50(5):1251–1257.
- 801 **Helmstetter CE**, Cooper S. DNA synthesis during the division cycle of rapidly growing *Escherichia coli* Br. *Journal
 802 of Molecular Biology*. 1968 Feb; 31(3):507–518.
- 803 **Henkel SG**, Beek AT, Steinsiek S, Stagge S, Bettenbrock K, de Mattos MJT, Sauter T, Sawodny O, Ederer M. Basic
 804 Regulatory Principles of *Escherichia coli*'s Electron Transport Chain for Varying Oxygen Conditions. *PLoS ONE*.
 805 2014 Sep; 9(9):e107640. doi: [10.1371/journal.pone.0107640](https://doi.org/10.1371/journal.pone.0107640).
- 806 **Ingledeow WJ**, Poole RK. The Respiratory Chains of *Escherichia coli*. *Microbiological Reviews*. 1984; 48(3):222–271.
 807 doi: [10.1128/MMBR.48.3.222-271.1984](https://doi.org/10.1128/MMBR.48.3.222-271.1984).
- 808 **Ireland WT**, Beeler SM, Flores-Bautista E, Belliveau NM, Sweredoski MJ, Moradian A, Kinney JB, Phillips R.
 809 Deciphering the Regulatory Genome of *Escherichia coli*, One Hundred Promoters at a Time. *bioRxiv*. 2020 Jan;
 810 doi: [10.1101/2020.01.18.910323](https://doi.org/10.1101/2020.01.18.910323).
- 811 **Jacob F**, Monod J. Genetic Regulatory Mechanisms in the Synthesis of Proteins. *Journal of Molecular Biology*.
 812 1961 Jun; 3(3):318–356. doi: [10.1016/S0022-2836\(61\)80072-7](https://doi.org/10.1016/S0022-2836(61)80072-7).
- 813 **Jensen RB**, Wang SC, Shapiro L. A moving DNA replication factory in *Caulobacter crescentus*. *The EMBO journal*.
 814 2001 Sep; 20(17):4952–4963.
- 815 **Jun S**, Si F, Pugatch R, Scott M. Fundamental Principles in Bacterial Physiology - History, Recent Progress, and
 816 the Future with Focus on Cell Size Control: A Review. *Reports on Progress in Physics*. 2018 May; 81(5):056601.
 817 doi: [10.1088/1361-6633/aaa628](https://doi.org/10.1088/1361-6633/aaa628).
- 818 **Kapanidis AN**, Margeat E, Laurence TA, Doose S, Ho SO, Mukhopadhyay J, Kortkhonja E, Mekler V, Ebright RH,
 819 Weiss S. Retention of Transcription Initiation Factor Σ 70 in Transcription Elongation: Single-Molecule Analysis.
 820 *Molecular Cell*. 2005 Nov; 20(3):347–356. doi: [10.1016/j.molcel.2005.10.012](https://doi.org/10.1016/j.molcel.2005.10.012).

- 821 **Khademi S**, O'Connell J, Remis J, Robles-Colmenares Y, Miercke LJW, Stroud RM. Mechanism of Ammonia
822 Transport by Amt/MEP/Rh: Structure of AmtB at 1.35 Å. *Science*. 2004 Sep; 305(5690):1587–1594. doi:
823 [10.1126/science.1101952](https://doi.org/10.1126/science.1101952).
- 824 **Khademian M**, Imlay JA. *Escherichia coli* Cytochrome c Peroxidase Is a Respiratory Oxidase That Enables the
825 Use of Hydrogen Peroxide as a Terminal Electron Acceptor. *Proceedings of the National Academy of Sciences*.
826 2017 Aug; 114(33):E6922–E6931. doi: [10.1073/pnas.1701587114](https://doi.org/10.1073/pnas.1701587114).
- 827 **Kraemer JA**, Sanderlin AG, Laub MT. The Stringent Response Inhibits DNA Replication Initiation in *E. coli* by
828 Modulating Supercoiling of oriC. *mBio*. 2019 Aug; 10(4):822.
- 829 **Li GW**, Burkhardt D, Gross C, Weissman JS. Quantifying Absolute Protein Synthesis Rates Reveals Principles
830 Underlying Allocation of Cellular Resources. *Cell*. 2014 Apr; 157(3):624–635. doi: [10.1016/j.cell.2014.02.033](https://doi.org/10.1016/j.cell.2014.02.033).
- 831 **Liu M**, Durfee T, Cabrera JE, Zhao K, Jin DJ, Blattner FR. Global Transcriptional Programs Reveal a Carbon Source
832 Foraging Strategy by *Escherichia coli*. *Journal of Biological Chemistry*. 2005 Apr; 280(16):15921–15927. doi:
833 [10.1074/jbc.M414050200](https://doi.org/10.1074/jbc.M414050200).
- 834 **Lu D**, Grayson P, Schulten K. Glycerol Conductance and Physical Asymmetry of the *Escherichia coli* Glycerol
835 Facilitator GlpF. *Biophysical Journal*. 2003 Nov; 85(5):2977–2987. doi: 10.1016/S0006-3495(03)74718-3.
- 836 **Lynch M**, Marinov GK. The Bioenergetic Costs of a Gene. *Proceedings of the National Academy of Sciences*.
837 2015 Dec; 112(51):15690–15695. doi: [10.1073/pnas.1514974112](https://doi.org/10.1073/pnas.1514974112).
- 838 **MaaløeO**. Regulation of the Protein-Synthesizing Machinery—Ribosomes, tRNA, Factors, and So On. Goldberger
839 R, editor, *Gene Expression*, Springer; 1979.
- 840 **Milo R**, Jorgensen P, Moran U, Weber G, Springer M. BioNumbers—the Database of Key Numbers in Molecular
841 and Cell Biology. *Nucleic Acids Research*. 2010 Jan; 38(suppl_1):D750–D753. doi: 10.1093/nar/gkp889.
- 842 **Monod J**. The Phenomenon of Enzymatic Adaptation and Its Bearings on Problems of Genetics and Cellular
843 Differentiation. *Growth Symposium*. 1947; 9:223–289.
- 844 **Mooney RA**, Darst SA, Landick R. Sigma and RNA Polymerase: An On-Again, Off-Again Relationship? *Molecular
845 Cell*. 2005 Nov; 20(3):335–345. doi: [10.1016/j.molcel.2005.10.015](https://doi.org/10.1016/j.molcel.2005.10.015).
- 846 **Mooney RA**, Landick R. Tethering Σ 70 to RNA Polymerase Reveals High in Vivo Activity of σ Factors and Σ 70-
847 Dependent Pausing at Promoter-Distal Locations. *Genes & Development*. 2003 Nov; 17(22):2839–2851. doi:
848 [10.1101/gad.1142203](https://doi.org/10.1101/gad.1142203).
- 849 **Neidhardt FC**, Ingraham JL, Schaechter M. *Physiology of the Bacterial Cell - A Molecular Approach*, vol. 1.
850 Elsevier; 1991.
- 851 **Ojkic N**, Serbanescu D, Banerjee S. Surface-to-volume scaling and aspect ratio preservation in rod-shaped
852 bacteria. *eLife*. 2019 Aug; 8:642.
- 853 **Patrick M**, Dennis PP, Ehrenberg M, Bremer H. Free RNA Polymerase in *Escherichia coli*. *Biochimie*. 2015 Dec;
854 119:80–91. doi: [10.1016/j.biochi.2015.10.015](https://doi.org/10.1016/j.biochi.2015.10.015).
- 855 **Peebo K**, Valgepea K, Maser A, Nahku R, Adamberg K, Vilu R. Proteome Reallocation in *Escherichia coli* with
856 Increasing Specific Growth Rate. *Molecular BioSystems*. 2015; 11(4):1184–1193. doi: 10.1039/C4MB00721B.
- 857 **Perdue SA**, Roberts JW. σ^{70} -Dependent Transcription Pausing in *Escherichia coli*. *Journal of Molecular Biology*.
858 2011 Oct; 412(5):782–792. doi: [10.1016/j.jmb.2011.02.011](https://doi.org/10.1016/j.jmb.2011.02.011).
- 859 **Phillips R**. Membranes by the Numbers. In: *Physics of Biological Membranes* Cham: Springer, Cham; 2018.p.
860 73–105.
- 861 **Ramos S**, Kaback HR. The Relation between the Electrochemical Proton Gradient and Active Transport in
862 *Escherichia coli* Membrane Vesicles. *Biochemistry*. 1977 Mar; 16(5):854–859. doi: 10.1021/bi00624a007.
- 863 **Roller BRK**, Stoddard SF, Schmidt TM. Exploiting rRNA operon copy number to investigate bacterial reproductive
864 strategies. *Nature microbiology*. 2016 Sep; 1(11):1–7.
- 865 **Rosenberg H**, Gerdes RG, Chegwidden K. Two Systems for the Uptake of Phosphate in *Escherichia coli*. *Journal
866 of Bacteriology*. 1977 Aug; 131(2):505–511.

- 867 **Rudd SG**, Valerie NCK, Helleday T. Pathways Controlling dNTP Pools to Maintain Genome Stability. *DNA Repair*.
 868 2016 Aug; 44:193–204. doi: [10.1016/j.dnarep.2016.05.032](https://doi.org/10.1016/j.dnarep.2016.05.032).
- 869 **Sánchez-Romero MA**, Molina F, Jiménez-Sánchez A. Organization of Ribonucleoside Diphosphate Reductase
 870 during Multifork Chromosome Replication in *Escherichia coli*. *Microbiology*. 2011 Aug; 157(8):2220–2225. doi:
 871 [10.1099/mic.0.049478-0](https://doi.org/10.1099/mic.0.049478-0).
- 872 **Schaechter M**, Maaløe O, Kjeldgaard NO. Dependency on Medium and Temperature of Cell Size and Chemical
 873 Composition during Balanced Growth of *Salmonella typhimurium*. *Microbiology*. 1958 Dec; 19(3):592–606.
- 874 **Schmidt A**, Kochanowski K, Vedelaar S, Ahrné E, Volkmer B, Callipo L, Knoops K, Bauer M, Aebersold R, Heine-
 875 mann M. The Quantitative and Condition-Dependent *Escherichia coli* Proteome. *Nature Biotechnology*. 2016
 876 Jan; 34(1):104–110. doi: [10.1038/nbt.3418](https://doi.org/10.1038/nbt.3418).
- 877 **Scott M**, Gunderson CW, Mateescu EM, Zhang Z, Hwa T. Interdependence of cell growth and gene expression:
 878 origins and consequences. *Science*. 2010 Nov; 330(6007):1099–1102.
- 879 **Sekowska A**, Kung HF, Danchin A. Sulfur Metabolism in *Escherichia coli* and Related Bacteria: Facts and Fiction.
 880 *Journal of Molecular Microbiology and Biotechnology*. 2000; 2(2):34.
- 881 **Shi H**, Bratton BP, Gitai Z, Huang KC. How to Build a Bacterial Cell: MreB as the Foreman of E. Coli Construction.
 882 *Cell*. 2018 Mar; 172(6):1294–1305. doi: [10.1016/j.cell.2018.02.050](https://doi.org/10.1016/j.cell.2018.02.050).
- 883 **Si F**, Le Treut G, Sauls JT, Vadia S, Levin PA, Jun S. Mechanistic Origin of Cell-Size Control and Homeostasis in
 884 Bacteria. *Current Biology*. 2019 Jun; 29(11):1760–1770.e7. doi: [10.1016/j.cub.2019.04.062](https://doi.org/10.1016/j.cub.2019.04.062).
- 885 **Si F**, Li D, Cox SE, Sauls JT, Azizi O, Sou C, Schwartz AB, Erickstad MJ, Jun Y, Li X, Jun S. Invariance of Initiation Mass
 886 and Predictability of Cell Size in *Escherichia coli*. *Current Biology*. 2017 May; 27(9):1278–1287.
- 887 **Sirk A**, Zatyka M, Sadowy E, Hulanicka D. Sulfate and Thiosulfate Transport in *Escherichia coli* K-12: Evidence
 888 for a Functional Overlapping of Sulfate- and Thiosulfate-Binding Proteins. *Journal of Bacteriology*. 1995 Jul;
 889 177(14):4134–4136. doi: [10.1128/jb.177.14.4134-4136.1995](https://doi.org/10.1128/jb.177.14.4134-4136.1995).
- 890 **Soler-Bistué A**, Aguilar-Pierlé S, Garcia-Garcera M, Val ME, Sismeiro O, Varet H, Sieira R, Krin E, Skovgaard O,
 891 Comerci DJ, Eduardo P C Rocha, Mazel D. Macromolecular crowding links ribosomal protein gene dosage to
 892 growth rate in *Vibrio cholerae*. *BMC Biology*. 2020 Dec; 18(1):1–18.
- 893 **Stasi R**, Neves HI, Spira B. Phosphate Uptake by the Phosphonate Transport System PhnCDE. *BMC Microbiology*.
 894 2019 Apr; 19. doi: [10.1186/s12866-019-1445-3](https://doi.org/10.1186/s12866-019-1445-3).
- 895 **Stevenson BS**, Schmidt TM. Life History Implications of rRNA Gene Copy Number in *Escherichia coli*. *Applied
 896 and Environmental Microbiology*. 2004 Nov; 70(11):6670–6677. doi: [10.1128/AEM.70.11.6670-6677.2004](https://doi.org/10.1128/AEM.70.11.6670-6677.2004).
- 897 **Stouthamer AH**. A Theoretical Study on the Amount of ATP Required for Synthesis of Microbial Cell Material.
 898 Antonie van Leeuwenhoek. 1973 Dec; 39(1):545–565. doi: [10.1007/BF02578899](https://doi.org/10.1007/BF02578899).
- 899 **Stouthamer AH**, Bettenhausen CW. A continuous culture study of an ATPase-negative mutant of *Escherichia coli*.
 900 *Archives of Microbiology*. 1977 Jun; 113(3):185–189.
- 901 **Svenningsen SL**, Kongstad M, Stenum TS, Muñoz-Gómez AJ, Sørensen MA. Transfer RNA Is Highly Unstable
 902 during Early Amino Acid Starvation in *Escherichia coli*. *Nucleic Acids Research*. 2017 Jan; 45(2):793–804. doi:
 903 [10.1093/nar/gkw1169](https://doi.org/10.1093/nar/gkw1169).
- 904 **Szenk M**, Dill KA, de Graff AMR. Why Do Fast-Growing Bacteria Enter Overflow Metabolism? Testing the
 905 Membrane Real Estate Hypothesis. *Cell Systems*. 2017 Aug; 5(2):95–104. doi: [10.1016/j.cels.2017.06.005](https://doi.org/10.1016/j.cels.2017.06.005).
- 906 **Taheri-Araghi S**, Bradde S, Sauls JT, Hill NS, Levin PA, Paulsson J, Vergassola M, Jun S. Cell-size control and
 907 homeostasis in bacteria. - PubMed - NCBI. *Current Biology*. 2015 Feb; 25(3):385–391.
- 908 **Tatusov RL**, Galperin MY, Natale DA, Koonin EV. The COG database: a tool for genome-scale analysis of protein
 909 functions and evolution. *Nucleic Acids Research*. 2000 Jan; 28(1):33–36.
- 910 **Taymaz-Nikerel H**, Borujeni AE, Verheijen PJT, Heijnen JJ, van Gulik WM. Genome-Derived Minimal
 911 Metabolic Models for *Escherichia coli* MG1655 with Estimated in Vivo Respiratory ATP Stoichiometry.
 912 *Biotechnology and Bioengineering*. 2010; 107(2):369–381. doi: [10.1002/bit.22802](https://doi.org/10.1002/bit.22802), _eprint:
 913 <https://onlinelibrary.wiley.com/doi/pdf/10.1002/bit.22802>.

- 914 **The Gene Ontology Consortium.** The Gene Ontology Resource: 20 years and still GOing strong. Nucleic Acids
915 Research. 2018 Nov; 47(D1):D330–D338.
- 916 **Valgepea K, Adamberg K, Seiman A, Vilu R.** *Escherichia coli* Achieves Faster Growth by Increasing Catalytic and
917 Translation Rates of Proteins. Molecular BioSystems. 2013; 9(9):2344. doi: 10.1039/c3mb70119k.
- 918 **Weber J, Senior AE.** ATP Synthesis Driven by Proton Transport in F1F0-ATP Synthase. FEBS Letters. 2003;
919 545(1):61–70. doi: 10.1016/S0014-5793(03)00394-6.
- 920 **Willsky GR, Bennett RL, Malamy MH.** Inorganic Phosphate Transport in *Escherichia coli*: Involvement of Two
921 Genes Which Play a Role in Alkaline Phosphatase Regulation. Journal of Bacteriology. 1973 Feb; 113(2):529–
922 539.
- 923 **Zhang L, Jiang W, Nan J, Almqvist J, Huang Y.** The *Escherichia coli* CysZ Is a pH Dependent Sulfate Transporter That
924 Can Be Inhibited by Sulfite. Biochimica et Biophysica Acta (BBA) - Biomembranes. 2014 Jul; 1838(7):1809–1816.
925 doi: 10.1016/j.bbamem.2014.03.003.
- 926 **Zhang Z, Aboulwafa M, Saier MH.** Regulation of Crp Gene Expression by the Catabolite Repressor/Activator,
927 Cra, in *Escherichia coli*. Journal of Molecular Microbiology and Biotechnology. 2014; 24(3):135–141. doi:
928 10.1159/000362722.
- 929 **Zhu M, Dai X.** Growth suppression by altered (p)ppGpp levels results from non-optimal resource allocation in
930 *Escherichia coli*. Nucleic Acids Research. 2019 Mar; 47(9):4684–4693.